Saracatinib, a Selective Src Kinase Inhibitor, Blocks Fibrotic Responses in *In Vitro, In Vivo* and *Ex Vivo* Models of Pulmonary Fibrosis

Authors

Farida Ahangari M.D.[1] †*, Christine Becker Ph.D.[3,4] †, Daniel G. Foster B.S.[2], Maurizio Chioccioli Ph.D.[1], Meghan Nelson M.S.[2], Keriann Beke B.S.[2], Xing Wang Ph.D.[3,4], Benjamin Readhead M.B.B.S.[3,5], Carly Meador B.S.[2], Kelly Correll B.S.[2], Loukia Lili Ph.D.[3], Helen M. Roybal M.S.[2], Kadi-Ann Rose B.S.[1], Shuizi Ding M.D.[1], Thomas Barnthaler M.D,Ph.D.[1,9], Natalie Briones M.S.[2], Giuseppe Deluliis B.S.[1], Jonas C. Schupp M.D.[1], Qin Li Ph.D.[1], Norihito Omote M.D.,Ph.D[1], Yael Aschner M.D.[2], Katrina W. Kopf M.S.,D.V.M[2], Björn Magnusson Ph.D.[6], Ryan Hicks Ph.D.[7], Anna Backmark M.S. [6], Leslie P. Cousens Ph.D.[8], Joel T. Dudley Ph.D.[3], Naftali Kaminski M.D.[1] †*, Gregory P. Downey M.D.[2] †*

Affiliations

[1] Section of Pulmonary, Critical Care, and Sleep Medicine, Department of Medicine, Yale University School of Medicine; New Haven, CT, USA

[2] Division of Pulmonary, Critical Care, and Sleep Medicine, Departments of Medicine, Pediatrics, and Immunology and Genomic Medicine, National Jewish Health, Denver, CO, USA

[2] Division of Pulmonary Sciences and Critical Care Medicine; Departments of Medicine and Immunology and Microbiology, University of Colorado, Aurora, CO, USA

[3] Institute for Next Generation Healthcare, Department of Genetics and Genomic Sciences. Icahn School of Medicine at Mount Sinai, New York, NY, USA

25 [4] Division of Clinical Immunology, Department of Medicine, Icahn School of Medicine at Mount

26 Sinai, New York, NY, USA

27 [5] ASU-Banner Neurodegenerative Disease Research Center, Arizona State University, Tempe, AZ,

28 USA

29 [6] Discovery Biology, Discovery Sciences, R&D, AstraZeneca, Gothenburg, Sweden

30 [7] BioPharmaceuticals R&D Cell Therapy, Research and Early Development, Cardiovascular,

31 Renal and Metabolism (CVRM), BioPharmaceuticals R&D, AstraZeneca, Gothenburg, Sweden

32 [8] Emerging Innovations, Discovery Sciences, R&D, AstraZeneca, Boston, MA, USA

33 [9] Section of Pharmacology, Otto Loewi Research Center, Medical University of Graz, Graz,

34 Austria

35 †These authors contributed equally to this work.

36

37 * Corresponding authors:

38 Gregory P. Downey, M.D.

39 Email: downeyg@njhealth.org, Phone:303-398-1436, Fax: 303-270-2243

40 Naftali Kaminski, M.D.

41 Email: naftali.kaminski@yale.edu, Phone: 203-737-4612, Fax: 203-785-3826

42 Farida Ahangari, M.D.

43 Email: farida.ahangari@yale.edu, Phone: 203-737-3559, Fax:203-785-6094

44
45

2

Abstract

Idiopathic Pulmonary Fibrosis (IPF) is a chronic, progressive, and often fatal disorder. Two FDA approved anti-fibrotic drugs, nintedanib and pirfenidone, slow the rate of decline in lung function, but responses are variable and side effects are common. Using an *in-silico* data-driven approach, we identified a robust connection between the transcriptomic perturbations in IPF disease and those induced by saracatinib, a selective Src kinase inhibitor, originally developed for oncological indications. Based on these observations, we hypothesized that saracatinib would be effective at attenuating pulmonary fibrosis. We investigated the anti-fibrotic efficacy of saracatinib relative to nintedanib and pirfenidone in three preclinical models: (i) *in vitro* in normal human lung fibroblasts (NHLFs); (ii) *in vivo* in bleomycin and recombinant adenovirus transforming growth factor-beta (Ad-TGF-β) murine models of pulmonary fibrosis; and (iii) *ex vivo* in precision cut lung slices from these mouse models. In each model, the effectiveness of saracatinib in blocking fibrogenic responses was equal or superior to nintedanib and pirfenidone.

3

Introduction

Idiopathic pulmonary fibrosis (IPF) is a chronic, relentless, and ultimately fatal disorder characterized by progressive scarring (fibrosis) of the lung parenchyma (1-3). The median survival for IPF patients is three years from diagnosis with most patients dying from respiratory failure due to disease progression (4). The overall prevalence of IPF worldwide and in United States ranges from 3.3-45.1, and 14.0 - 63.0 cases per 100,000 respectively*(4-6)*. Recent studies suggest that both the prevalence of, and mortality from, IPF are increasing *(4, 7)*.

The mechanisms driving pulmonary fibrosis remain incompletely understood and both genetic and environmental factors appear to be important in disease pathogenesis *(8, 9)*. A widely accepted hypothesis is that, in genetically susceptible individuals, the lung is repeatedly injured (via an unknown cause) and aberrant repair provokes release and activation of fibrogenic mediators, myofibroblast accumulation, and deposition of excess extracellular matrix (ECM) resulting in progressive fibrosis *(10-12)*. Cellular responses to profibrotic mediators are frequently transduced through transmembrane receptors via intracellular signaling pathways that are controlled in part by Src family tyrosine kinases (SFK) that include Src, Yes, Fyn, Fgr, Lck, Hck, Blk, Lyn, and Frk *(13, 14)*. SFK are involved in a range of signaling pathways essential for cellular homeostasis such as proliferation, differentiation, motility, adhesion, and cytoskeletal organization. Studies in preclinical models of IPF suggest that several Src-dependent processes contribute to IPF pathogenesis, including myofibroblast differentiation and fibrogenic gene expression *(15, 16)*.

Treatment of IPF remains suboptimal. Two anti-fibrotic drugs, pirfenidone (Esbriet[®]) and nintedanib (OFEV[®]), were approved by the FDA in 2014 for the treatment of IPF *(17-19)*. Clinical trials and real-world experience demonstrate that, while on average, both drugs slow the rate of

4

93   decline in lung function, responses are variable, and these drugs neither cure IPF nor improve the

94   major symptoms including cough and dyspnea *(20, 21)*. Thus, there remains an urgent need for

95   development of more effective therapies that safely modify the course of IPF and restore quality of

96   life.

97   An evolving understanding of the molecular underpinnings of human diseases has provided

98   opportunities to precisely target disease-specific pathways using bioinformatic methods to mine

99   genomic, molecular, and clinical data *(22-24)*. This approach has been used successfully to identify

100   connections between disease and drug 'molecular signatures', revealing opportunities to use

101   existing drugs in new therapeutic areas ('computational drug repurposing') *(22-25)*. As part of a

102   data-driven approach to repurpose Phase-II ready compounds for new diseases (*26*), we identified

103   saracatinib as a potential therapeutic compound for IPF. Saracatinib is a potent and selective Src

104   kinase inhibitor, originally developed for oncological indications *(27-29)*. Building on the initial

105   insights gleaned from transcriptomic connections, and the evidence strongly supporting a pivotal

106   role for Src kinase in IPF pathophysiology, we sought to determine the anti-fibrotic efficacy of

107   saracatinib relative to nintedanib and pirfenidone in pre-clinical cell culture and animal models of

108   IPF and to elucidate the molecular signatures of pathological fibrogenesis and drug responsiveness.

109

110   **Results**

111   ***Computational drug re-purposing approach identifies a connection between saracatinib and***

112   ***IPF***

113   At the outset, we undertook a disease agnostic, data-driven approach to explore novel

114   connections between diseases and compounds previously tested in clinical studies. A set of 32

115   compounds was selected for this analysis based on a combination of factors that included

5

116   experience in Phase 1 and Phase 2 clinical studies and potential for further clinical development

117   beyond the disease for which the compound was originally designed ('drug repositioning')

118   (https://openinnovation.astrazeneca.com/data-library.html#transcriptomicprofilingdata) (*26*). The

119   method applied was based on a modified connectivity mapping approach *(26, 31, 32)* where the

120   transcriptomic signature of each compound was compared computationally with transcriptomic

121   signatures of human diseases. Briefly, differential gene expression signatures for each compound

122   were generated by preforming RNA sequencing on two different cell lines (A549 and MCF7) after

123   exposure to two concentrations of each of the 32 compounds (e.g., "Compound-A A549 High

124   dose", "Compound-A MCF7 High dose", "Compound-A A549 Low dose", "Compound-A MCF7

125   Low dose"). This analysis was done blinded to the compound identity or chemistry and was

126   generated using the genome-wide pattern of mRNA changes in cell-matched compound-versus

127   vehicle-treated samples. **(Figure 1A)**. A disease transcriptomic library, consisting of over 700

128   unique disease signatures, was built from publicly available gene expression data *(23, 33)*. To

129   identify novel clinical indications for each compound, a "connectivity score" was calculated by

130   comparing each disease signature to each compound signature. The connectivity score aims to

131   summarize the transcriptomic relationship between each compound and disease, such that a strongly

132   negative score indicates that the compound will induce transcriptomic changes that may revert or

133   "normalize" the disease signature *(31)*. Using this method, significant negative connectivity scores

134   were found between the Src kinase inhibitor, saracatinib, and IPF disease signatures derived from

135   patient lung biopsies (GSE24206) *(34)* and cultured fibroblasts (GSE44723) *(35)* (FDR <0.01),

136   **(Table-S1)**.

137   Accordingly, we performed a disease enrichment analysis (DEA), with the goal of identifying

138   high-level disease categories that are transcriptomically connected to saracatinib. This analysis

6

139   identified that IPF disease signatures were highly over-represented in connecting with saracatinib

140   **(Figure 1B)**, indicating that saracatinib is globally relevant to IPF disease.

141   In order to probe the biology driving the connection between saracatinib and the IPF

142   signatures, we conducted a leading-edge enrichment analysis to identify over-represented gene

143   sets that point to pathways by which saracatinib may affect IPF disease. This analysis identified

144   numerous gene sets including interferon gamma (IFNγ) response, epithelial-mesenchymal

145   transition (EMT), and tumor necrosis factor alpha (TNFα) signaling pathways, all of which have

146   been implicated in the pathogenesis of IPF. Additionally, Kinase Enrichment Analysis (KEA) of

147   these data identified enrichments for receptor-interacting serine/threonine-protein kinase 3

148   (RIPK3) along with multiple members of the mitogen activated protein (MAP) kinase family

149   **(Table 1)**.

150   To clarify if this connectivity was a feature among other Src inhibitors or unique to

151   saracatinib, we used data from the previously published connectivity Map, a collection of publicly

152   available expression data from cultured human cells treated with small molecules *(32)*. This data

153   collection contains transcriptomic data in a range of experimental conditions for saracatinib as well as

154   other Src kinase inhibitors. This resource also includes data from the two IPF FDA-approved drugs

155   pirfenidone and nintedanib. We compared each of these drug signatures to the IPF disease signatures

156   in our disease library. One of the IPF disease signatures connected significantly with all 6 compounds

157   (saracatinib, dasatinib, bosutinib, pirfenidone, nintedanib and NM-PP1) and the strongest connection

158   was with saracatinib **(Figure 1C)**. In summary, using complementary bioinformatics approaches, we

159   identified a robust transcriptomic connection between saracatinib and IPF thus providing a strong

160   foundation for the hypothesis that saracatinib might have a potential therapeutic benefit in IPF.

161   ***Saracatinib inhibits TGF-β–induced phenotypic changes in human lung fibroblasts, (In vitro)***

162   As the compound signature was derived from initial cell screening with a computational

163   approach, we next investigated the effects of saracatinib in a more disease-relevant setting to

164   confirm the connection between saracatinib and IPF. We assessed the effect of saracatinib on

165   TGF-β-induced fibrogenic processes in cultured primary normal human lung fibroblasts (NHLF)

166   to study signaling pathways relevant to human IPF disease. We confirmed that, TGF-β stimulation

167   induces a significant increase in Src phosphorylation of Y416, a response that correlates with

168   activation of Src kinase activity(*36*) **(Figure S1A and S1B).** It has been well demonstrated that

169   saracatinib treatment efficiently inhibits TGF-β–induced Src kinase activity in these cells(*16*). We

170   chose to compare the effect of saracatinib to the two FDA-approved anti-fibrotic drugs, nintedanib

171   and pirfenidone in this *in vitro* system. We carefully selected the optimum dose for all three

172   compounds based on the established clinically relevant doses(*37, 38*) and our initial screening

173   experiments **(Figure S2A and S2B)**. We observed that saracatinib significantly inhibited TGF-β-

174   induced expression of many profibrotic genes including *ACTA2*, *COL1A1* and *SERPIN1* to a

175   similar or greater extent than that observed for nintedanib or pirfenidone **(Figure 2A, 2B and 2C)**.

176   To validate this finding, we repeated the experiment in primary human lung fibroblasts isolated

177   from three different donors and confirmed the consistency of these findings across all three donors

178   **(Figure S3A and S3B)**. We next compared the effects of the three drugs on TGF-β-induced Smad3

179   phosphorylation in NHLF, as a readout of canonical TGF-β fibrogenic signaling. Saracatinib, but

180   not nintedanib nor pirfenidone, significantly inhibited TGF-β-induced Smad3 phosphorylation

181   **(Figure 2D)**. We extended our investigation by comparing the effects of saracatinib to the other

182   two drugs on TGF-β-induced morphological changes in human fibroblasts. Confocal

183   immunofluorescence imaging of these cells for alpha smooth muscle actin (α-SMA) and

184   filamentous actin (F-actin) demonstrated a strong inhibitory effect of saracatinib on TGF-β-

8

185 induced alterations in cell shape and stress fiber formation characteristic of myofibroblast

186 transformation (fold change >2, p-value ≤0.001), **(representative images, Figure 2E)** and

187 **(quantifications, Figure 2F and 2G)**. Nintedanib exhibited a similar, but less potent, inhibitory

188 response compared to saracatinib on these TGF-β induced phenotypic changes. Concordant with

189 our earlier findings, pirfenidone did not show any effects on TGF-β induced structural changes in

190 human lung fibroblasts.

191   To extend these observations and investigate the broader effects of saracatinib in this

192 disease-relevant *in vitro* model, we generated transcriptomic drug signatures by performing bulk

193 RNA sequencing (RNAseq) on NHLF cells treated with saracatinib, nintedanib, pirfenidone, or

194 vehicle control in the presence or absence of TGF-β stimulation. We identified that saracatinib

195 altered expression of over 500 individual genes (adj. p-value <0.05) in TGF-β treated cells **(Figure**

196 **2H)**. We carried out gene set enrichment analysis (GSEA) with the goal of identifying gene sets

197 that were significantly over-represented. This analysis revealed that saracatinib induced alterations

198 in numerous pathways identified from the Hallmark and KEGG databases, with IFNα, IFNγ, EMT,

199 and inflammatory responses among the top pathways **(Figure 2I** and **Table S2)**. We next identified

200 the transcriptomic effects that were unique to saracatinib and could be used to differentiate the

201 effects of saracatinib from nintedanib and pirfenidone **(Figure S4A and S4B)**. GSEA suggested

202 that both nintedanib and saracatinib target several common gene sets including IFNγ, IFNα, and

203 inflammatory responses. Gene sets that were uniquely enriched by saracatinib included EMT,

204 TGF-β and WNT signaling while gene sets that were uniquely enriched by nintedanib related

205 predominantly to metabolism. In summary, saracatinib inhibits TGF-β–induced fibrogenic

206 responses in this *in vitro* system more effectively than nintedanib and pirfenidone.

207 ***Saracatinib inhibits pulmonary fibrosis in preclinical animal models, (In vivo)***

208   Next, we compared the effects of saracatinib, nintedanib and pirfenidone at clinically

209   relevant doses (*39-43*), in two preclinical models of pulmonary fibrosis in mice (*44, 45*). In the

210   first model, fibrosis was induced using a single dose of bleomycin (1.5U/Kg) administered into

211   the lung by oropharyngeal aspiration (OPA) and mice received either saracatinib, nintedanib,

212   pirfenidone or vehicle control once daily via oral gavages on days 10-27 post-bleomycin

213   administration. On day 28, the mice were euthanized, lungs were harvested and the anti-fibrotic

214   effects of all three drugs were assessed. Mice receiving vehicle control exhibited prominent weight

215   loss as expected after the administration of bleomycin, while all drug-treated mice, except the mice

216   treated with pirfenidone, recovered their weight loss by the end of the experiment **(Figure S5A**

217   **and S5B)**. The bleomycin-induced increase in lung collagen content was significantly attenuated

218   in mice receiving saracatinib, nintedanib, or pirfenidone (p-value ≤0.001) **(Figure 3A).** Consistent

219   with the biochemical analysis, saracatinib significantly attenuated the bleomycin-induced whole

220   lung expression of fibrogenic genes including *Acta2, Col1a1*, and *Col3a1* **(Figure 3B, 3C** and

221   **S6A)**, (p-value ≤0.001 for *Acta* 2 and *Col3a1*, p-value ≤0.01 for *Col1a1*), whereas neither

222   nintedanib nor pirfenidone treatment resulted in any significant changes in the expression of these

223   fibrogenic genes. Histopathological evaluation of these lungs using Masson's Trichrome staining

224   demonstrated a greater reduction in bleomycin-induced pulmonary fibrosis by saracatinib and

225   nintedanib (p-value ≤0.001) compared to pirfenidone (p-value ≤0.01) **(representative images,**

226   **Figure 3D** and **quantifications, Figure 3E).** Micro-computerized tomography (CT) analysis of

227   these mice lungs supported the biochemical and histopathological observations; aerated lung

228   volume measurements showed saracatinib and nintedanib significantly attenuated the bleomycin-

229   induced radiographic alterations in lung parenchyma (p-value ≤0.001) and to a greater extent than

230   pirfenidone (p-value ≤0.01) **(representative images, Figures 3F, S7** and **quantifications, Figure,**

10

231 **3G)**. Finally, lung function measurements and physiological evaluation of these mouse lungs

232 identified that saracatinib also significantly attenuated bleomycin-induced alterations in lung

233 physiology [static compliance (Cst) and elastance] as measured using the flexiVent system (fold

234 change=2, p-value ≤0.001) compared to nintedanib or pirfenidone (p-value ≤0.01) **(Figure 3H)**.

235   A second model of pulmonary fibrosis was established using expression of recombinant

236 murine TGF-β using adenoviral-mediated gene delivery (Ad-TGF-β) administered to the lung

237 intranasally. As in the bleomycin model, all the three drugs were given to mice once daily via oral

238 gavages from days 10-27 after TGF-β administration. Similar to the bleomycin model, mice

239 receiving vehicle control exhibited prominent weight loss after the administration of TGF-β

240 adenovirus, but notably, only the mice treated with saracatinib recovered their weight loss by the

241 end of the experiment **(Figure S3C** and **S3D)**. In this model, only saracatinib demonstrated

242 antifibrotic effects as assessed by a reduction in lung collagen content (p-value≤ 0.001) **(Figure

243 3I)** and expression of *Acta2*, *Col1a1* and *Col3a1* mRNA (p-value ≤ 0.001) **(Figure 3J** and **3K and

244 S6B)**. By contrast, neither nintedanib nor pirfenidone attenuated fibrosis in this model.

245 Histopathological assessment of the lungs using Masson's Trichrome and α-SMA staining

246 confirmed these observations **(representative images, Figure 3L, 3M, S8A** and **S8B** and

247 **quantification**, **Figure 3N** and **3O)**.

248   Given the fact that TGF-β signaling cascades are consistently activated in fibrotic tissues,

249 regardless of the etiology of the initial injury and that Smad3 pathway is a key intermediary in this

250 cascade (*46, 47*), we evaluated the effect of saracatinib on Smad3 phosphorylation in the lung

251 tissues after bleomycin and Ad-TGF-β treatment. We identified significant inhibition of this

252 pathway by saracatinib in both preclinical animal models of pulmonary fibrosis **(Figure S9A-D)**.

11

253   In summary, in two complementary preclinical mouse models of IPF, saracatinib

254   attenuated experimental pulmonary fibrosis significantly more effectively than pirfenidone or

255   nintedanib at clinically relevant doses.

Saracatinib inhibits lung fibrosis in precision cut lung slices (ex vivo model)

257   We next sought to confirm these observations in an *ex vivo* model using precision cut lung

258   slices (PCLS) to compare the anti-fibrotic effects of saracatinib with nintedanib and pirfenidone

259   (*48*). PCLS is a useful method to test the therapeutic effects of different compounds in a relatively

260   preserved lung architecture containing various lung-resident cell types and ECM (*49*). In this

261   study, mice were treated with either bleomycin or Ad-TGF-β and euthanized at the peak of the

262   fibrotic response (day 14 for bleomycin and day 21 for Ad-TGF-β model). Lung slices were

263   prepared and treated *ex vivo* with each of the three drugs or vehicle for 5 days **(Figure 4A-L)**.

264   These lung slices remain viable at least for 5 days (120 hours), **(Figure S10)**. Quantitative RT-

265   PCR (qRT-PCR) analysis of lung slices revealed a dramatic reduction in *Col1a1* and *Acta2* mRNA

266   expression by saracatinib in PCLS harvested from mice treated with either bleomycin or Ad-TGF-

267   β (p-values≤0.001), while the fibrosis was sustained in the control groups (**Figure 4A** and **4B; 4G**

268   and **4H,** respectively**)**. Live serial imaging of the lung slices using second harmonic generation

269   microscopy (SHG) demonstrated that saracatinib significantly attenuated collagen accumulation

270   in both models (p-values≤0.001) **(representative images, Figure 4C** and **4I** and **quantifications,**

271   **Figure 4D** and **4J)**. Note that it was not possible to assess the effects of nintedanib on collagen

272   content by SHG in this model due to a strong auto-fluorescence signal generated by nintedanib.

273   Treatment with pirfenidone attenuated lung collagen content (p-values≤0.001) only in the TGF-β

274   model. Histological evaluation of the lung slices using Masson's Trichrome staining revealed that

275   saracatinib strongly attenuated lung fibrosis in both models (p-values≤0.001) **(representative**

12

276   **images, Figure 4E and 4K** and **quantifications, Figure 4F** and **4L)**. In summary, using PCLS as

277   a complementary model, saracatinib was more effective than either nintedanib or pirfenidone in

278   attenuating pulmonary fibrosis in an *ex vivo* model and confirmed our finding in the *in vivo* murine

279   models.

280   *Comparison of transcriptional changes in mouse models identifies core genes relevant for IPF*

281   *and points to a mechanism of action of saracatinib*

282   We undertook bioinformatic analysis to explore the transcriptional changes underlying the

283   observed anti-fibrotic effects of saracatinib in both murine models of pulmonary fibrosis. RNAseq

284   was carried out on lungs isolated from mice treated with either bleomycin or Ad-TGF-β in the

285   presence or absence of saracatinib treatment. Consistent with the favorable clinical safety profile

286   of saracatinib, there were relatively few gene expression changes in mice receiving saracatinib

287   alone compared to the control group. Importantly, saracatinib reversed the expression of many of

288   the genes that were altered by bleomycin **(Figure 5A and 5B)**. This was also reflected by pathway

289   analysis; GSEA demonstrated that saracatinib reversed alterations in numerous gene sets induced

290   by bleomycin (including Myc Targets, E2F Targets, EMT, and G2M Checkpoint gene sets)

291   **(Figure 5C)**. Analysis of the pulmonary transcriptional changes observed in the Ad-TGF-β model

292   revealed that TGF-β induced changes in approximately 4500 genes; however, contrary to the

293   observed changes in the bleomycin model, saracatinib treatment had a much smaller effect with

294   fewer significant changes in expression. Further evaluation using GSEA, taking expression levels

295   of all genes into account, demonstrated that saracatinib attenuated many pathways altered by TGF-

296   β expression including IFNγ, IL6, JAK-STAT3 signaling, and IFNα responses **(Figure 5D).**

297   As neither mouse model faithfully recapitulates all aspects of human IPF, we compared the

298   transcriptional changes observed in these two animal models and identified a set of genes common

13

299   to both models (consisting of 1233 upregulated genes and 1256 downregulated genes). A subset

300   of these genes is reversed by saracatinib (225 upregulated, 560 downregulated). To interrogate this

301   subset further, a protein-protein interaction network analysis identified modules including ECM

302   organization, immune system processes, ER-golgi transport and neutrophil degranulation **(Figure**

303   **S10)**. Within this ECM cluster are numerous known markers of fibrosis including members of the

304   collagen family (*Col3a1*, *Col4a1*, *Col4a2*, *Col5a2*, *Col12a1*, *Col16a1*), fibronectin (*Fn1*), laminin

305   (*Lama1*), tenascin (*Tnc*), fibrillin (*Fbn1*), TGF-β receptor1 (*TGF-βr1*) and the ECM receptor *Cd44*

306   **(Figure S11).**

307

308   **Discussion**

309   In this study, we used an innovative disease-agnostic computational biology-based

310   approach and identified the Src kinase inhibitor, saracatinib (AZD0530) *(29)*, as a potential

311   therapeutic agent for IPF and delineated multiple fibrogenic pathways targeted by this agent at the

312   molecular level. Further, we validated the efficacy of saracatinib in blocking fibrogenic responses

313   in several complementary pre-clinical models of pulmonary fibrosis. Our data provide strong

314   evidence that saracatinib is equal or superior to the two FDA-approved drugs, nintedanib and

315   pirfenidone at inhibiting pulmonary fibrosis in experimental models. Analysis of the

316   transcriptional changes induced by saracatinib in the *in vitro* and *in vivo* models of pulmonary

317   fibrosis demonstrated that saracatinib was able to reverse the expression of diverse fibrogenic

318   genes and pathways such as myofibroblast differentiation, EMT, ECM organization, immune

319   system processes, ER-golgi transport, and neutrophil degranulation. Importantly, many of these

320   differentially expressed gene sets and pathways are selectively modified by saracatinib as

321   compared to nintedanib and pirfenidone. Taken together, our data support the validity of a

14

322 transcriptomics-based bioinformatics approach to generate novel hypotheses for drug repurposing

323 in complex human diseases such as IPF.

324   At the inception of this study, we used genome-wide transcriptional profiling of human

325 IPF lungs cross-referenced with distinct drug transcriptomic signatures to identify Src kinase-

326 dependent signaling pathways as critical checkpoints that control pro-fibrotic responses in the

327 lung. Importantly, we established that saracatinib was a potent and effective therapeutic agent that

328 significantly attenuated experimental pulmonary fibrosis in several preclinical models with equal

329 or greater efficacy compared to the two FDA-approved drugs, nintedanib and pirfenidone. This

330 approach, anchored in transcriptomic profiles in human lung cells and tissues, led to identification

331 of novel pathways that are relevant to human IPF.

332   Our study provides additional information and is complementary to proteomic-based

333 analyses of human tissues that have yielded therapeutic targets for pulmonary fibrosis *(50)*. This

334 is of considerable practical importance because, despite massive investments made by academia

335 and industry, many drugs have failed in later stages of development, partly due to the poor

336 predictability of animal models in drug discovery that do not reflect human disease *(51, 52)*.

337 Repurposing drugs to treat conditions other than the one for which they were developed and/or

338 approved, can shorten timelines, decrease costs, and increase success rates. Using a computational

339 biology approach in combination with Connectivity Map (CMap) analysis will facilitate

340 identification of new drugs, predicting drug candidates, and discovering connections among small

341 molecules sharing a mechanism of action. Connectivity MAP analysis of single cell RNA

342 sequencing of bronchial brushings from IPF patients also suggested that gene expression changes

343 in   IPF   airway   basal   cells   can   be   reversed   by   SRC   inhibition,

344 (https://www.biorxiv.org/content/10.1101/2020.09.04.283408v1). Based on the connectivity

15

345 scores of saracatinib to IPF relative to nintedanib and pirfenidone using L1000 data, we identified

346 that saracatinib had greater connectivity to IPF than the other two FDA approved drugs. This

347 approach has been widely used as a resource in cancer drug discovery *(31, 53)* and our study

348 extends this methodology to IPF treatment.

349   Several studies have shown that SFK control key signaling pathways relevant to pulmonary

350 fibrosis pathogenesis *(54)* including TGF-β-mediated myofibroblast differentiation and fibrogenic

351 responses in lung fibroblasts *(16)*. SFK are also required for TGF-β-driven EMT and mediate TGF-

352 β-induced β-catenin phosphorylation, a critical determinant of fibrogenesis in alveolar epithelial

353 cells *(55)*. SFK are also necessary for the recruitment and activation of immune cells as well as

354 having other roles in pulmonary inflammation *(54)*. We have reported that mice genetically

355 deficient in protein tyrosine phosphatase (PTP)α, a known activator of SFK, are protected from

356 experimental pulmonary fibrosis (*56, 57*). We also reported that the SH2 domain–containing

357 tyrosine phosphatase2 (SHP2) is an antifibrotic regulator in pulmonary fibrosis (*58, 59*). These

358 studies underscore the importance of reversible tyrosine phosphorylation reactions, controlled by

359 specific tyrosine kinases and phosphatases, in the pathogenesis of pulmonary fibrosis and provide

360 a mechanistic foundation for the use of saracatinib in the treatment of pulmonary fibrosis.

361   Our studies using normal human lung fibroblasts provide strong evidence that saracatinib

362 inhibits TGF-β-induced fibrogenic responses, more potently than either nintedanib or pirfenidone,

363 at the levels of mRNA expression, post-translational signal transduction, and myofibroblast

364 morphological changes. We observed that saracatinib was more effective than nintedanib or

365 pirfenidone in animal models and in PCLS. Both models revealed that saracatinib perturbed

366 'EMT', 'MYC targets' and 'IL6_JAK_STAT signaling' gene sets and that saracatinib uniquely

367 induced perturbations in 'E2F target', 'G2M checkpoints' and 'oxidative phosphorylation' gene

16

368 sets in the bleomycin model, and interferon gene sets in the Ad-TGF-β model. This analysis

369 provides important insights into the mechanisms by which SFK modulate fibrogenic signaling

370 pathways. Further investigation into the precise mechanisms of saracatinib action in the context

371 of IPF is the subject of ongoing/future work.

372 Several questions of interest with respect to the effects of saracatinib on fibrogenic

373 pathways remain to be addressed. In the current study we focused on TGF-β-dependent pathways

374 because of the well accepted importance of this growth factor in organ fibrosis *(60, 61)*. In addition

375 to TGF-β, other growth factors including platelet-derived growth factor (PDGF) *(62, 63)*, insulin-

376 like growth factor-(IGF)1 *(64)* and fibroblast growth factors (FGFs) *(65)* are known to trigger pro-

377 fibrotic cellular responses through signaling pathways that are controlled by SFK. In future studies,

378 we plan to investigate the effects of saracatinib on PDGF, IGF-1, and FGF fibrogenic signaling.

379 Kinase Enrichment Analysis (KEA) of differentially expressed gene sets altered by

380 saracatinib identified enrichment for RIPK3 and the MAP Kinases. Importantly, RIPK3 has been

381 implicated in the pathogenesis of renal fibrosis *(66)*. SFK are known to regulate MAP Kinase-

382 dependent signaling pathways relevant to fibrogenesis *(67, 68)*. Whether RIPK3 is regulated by

383 SFK is unknown and the subject of current investigations.

384 In conclusion, based on a computational drug repurposing strategy, we have identified

385 saracatinib as a potential therapeutic for IPF. As the safety profile of saracatinib has previously

386 been established, the efficacy of saracatinib in IPF patients is now being investigated in a Phase

387 1b/2a clinical trial (NCT04598919). To our knowledge, this is the first study that has used a

388 computational approach to link a compound to a specific disease using a computational approach,

389 validated the efficacy of the drug in three complementary preclinical *in vitro*, *in vivo* and *ex vivo*

390 models and culminated in a human clinical trial in the treatment of IPF.

17

Materials and Methods

Reagents

Saracatinib was provided by AstraZeneca. Pirfenidone and nintedanib were purchased from Tocris Bioscience (Cat No. 1093) and Selleckchem (Cat No. S1010), respectively. Hydroxypropyl methyl Cellulose (HPMC) was purchased from Sigma (Cat No. P8074).

***In vitro* assays**

Experiments were performed using primary normal human lung fibroblasts (NHLF) from three different donors (Lonza) and all experiments were performed using cells of passages 3-5. All experiments were performed with 6 technical replicates and repeated at least three times.

TGF-β-induced Src activation: Normal Human Lung Fibroblasts were plated on rat tail collagen-coated non-tissue culture plastic, serum starved overnight, and then stimulated with human recombinant TGF-β (2 ng/ml) for 60 min at 37°C. Protein was solubilized in RIPA buffer and then subject to SDS-PAGE and immunoblotting with antibodies to total SRC and phospo-Y416 SRC (Cell Signaling, 2110 and 6943 respectively). Membranes were scanned using a Licor Odysey fluorescent imaging instrument and densitometry conducted using Image Studio Lite, N=6, ** P=0.0055.

Dose selection experiment: For choosing the optimal dose, cells were serum-starved overnight and then incubated with inhibitors at two selected clinically relevant doses (saracatinib: (0.12 & 0.3 μM), nintedanib: (0.1 &1 μM), pirfenidone: (10 and 20 μg/ml) or vehicle A (DMSO)) for 60 min followed by stimulation with human recombinant TGF-β1 (2 ng/ml) or vehicle B as control for 6 and 24 hours. After initial pilot experiments to identify optimal conditions, we selected clinically relevant concentrations for each drug [based on the known pharmacokinetic profile (Cmax) in humans available from the respective clinical development programs] and explored the

18

414   effects of all three compounds on fibrogenic responses to TGF-β in normal human fibroblasts.

415   Cells were serum-starved overnight and then incubated with inhibitors [saracatinib: 0.3 μM,

416   nintedanib: 1 μM, pirfenidone: 20 μg/ml or vehicle (DMSO)] for 60 min followed by stimulation

417   with human recombinant TGF-β (2 ng/ml) or vehicle control for the indicated times (30 min for

418   western blots, 24 hours for gene expression) in the continued presence of the inhibitors.

419   *Gene Expression Analysis:* For qPCR analysis, cells were lysed in Trizol, RNA was extracted

420   with miRNeasy Mini Kit from Qiagen. The levels of mRNA for the fibrogenic genes were

421   quantified by RT-qPCR and normalized to GAPDH expression.

422   *Western Blots:* For western blot, cells were lysed in RIPA buffer and analyzed by SDS-PAGE

423   followed by western blotting with antibodies to phospho and total Smad3 (Cell Signaling). The

424   blots were quantified using an Odyssey fluorescent imaging system.

425   *Immunofluorescence (IF) staining:* IF was performed 24 hours after the treatments, using anti-α-

426   SMA (ab5694, Abcam) with T-6778 anti-rabbit Ig-TRITC as a secondary antibody, along with F-

427   actin stain (Invitrogen- R37710), following the manufacturers' protocols. Imaging was conducted

428   by confocal microscopy (Leica SP5) and images were processed and quantified using Image J

429   software.

430   *In vivo* experiments

431   All animal procedures were approved by the Institutional Animal Care and Use

432   Committees (IACUC) from National Jewish Health and Yale University. Pulmonary fibrosis was

433   induced in C57Bl/6 mice by intrapulmonary delivery of bleomycin or recombinant adenovirus

434   TGF-β (Ad-TGF-β). Bleomycin (1.5 U/kg) or saline administered by oropharyngeal instillation

435   and Ad-TGF-β1 (VQAd CMV mTGF-β1-Viraquest), (2 x 10^9 pfu per mouse) or empty vector was

436   administered via the intranasal route. In both animal models, treatment with drugs was started on

19

437 day 10 and drugs were administered daily by oral gavage (saracatinib 20mg/kg; nintedanib

438 60mg/kg; pirfenidone 300mg/kg) until day 28. Mice were euthanized, and lungs were harvested

439 on day 28 for fibrosis analysis. Mice of both sexes were studied and 15-20 mice per group were

440 used.

441 *Hydroxyproline Assay:* Whole right lungs from each animal were used for hydroxyproline

442 measurements using Hydroxyproline Colorimetric Assay Kit (Biovision K555-100). Briefly,

443 constant weight homogenates from the mice lungs were hydrolyzed in 12 N HCl for 3 hrs at 120

444 °C. The dried digestions reacted with Chloramine T and were visualized by DMAB reagents. The

445 absorbance was measured at 560 nm in a microplate reader. Data were expressed as µg of

446 hydroxyproline/right lung.

447 *Gene Expression:* Left lungs were used for RNA extraction via miRNeasy Mini Kit (Qiagen-

448 217004) according to the manufacturer's instructions. The purity of the RNA was verified using a

449 NanoDrop at 260 nm, and the quality of the RNA was assessed using the Agilent 2100 Bioanalyzer

450 (Agilent Technologies). Purified RNA was used either for gene expression analysis by TaqMan

451 gene expression assays or RNAseq analysis.

452 *Histology:* Animal tissue sections from all the groups were stained with Masson's Trichrome

453 (collagen/connective tissue), H&E (Hematoxylin and Eosin stains) or α-SMA (alpha smooth

454 muscle). Immunostaining was performed after paraffin removal, hydration, and blocking,

455 following the recommendation of the manufacturer (ABC detection system from Vector lab,

456 USA). All sections were analyzed using a Nikon microscope. Quantification of collagen was done

457 with ImageJ software.

458 *MicroCT Analysis:* MicroCT scan was performed on live animals using Bruker SkyScan 1276

459 Desktop *In-Vivo* MicroCT System following the manufacturers' protocols. The microCT data from

20

460 all the mice lungs were analyzed using the computer program CT-Analyser (CTAn) by Bruker. In

461 brief, the CT scan is turned into a binary image and the threshold for what is considered aerated

462 lung tissue vs other tissues is chosen by the blinded person performing the data analysis. This

463 threshold is chosen based on closely matching the binary image of the scan to the actual scan. The

464 same threshold is then applied to each scan. With CTAn, an automatic series of computer

465 operations separates the aerated lung tissue from the rest of the mouse body, and this is quantitated

466 in mm^3. The Hounsfield Units are obtained with this same program from a calculation that is

467 based on a CT scan of distilled water serving as a standard for the CT scanner. Reconstructed scans

468 are corrected for misalignment, ring artifact, and beam hardening. The same beam hardening, and

469 ring artifact corrections are applied to all scans. The misalignment is unique for each scan. This is

470 done with NRecon from Bruker. The detailed explanation of aerated lung volume calculation

471 includes a) Turn image into binary image and set ROI (region of interest) as the mouse body. b)

472 Reload original image with new ROI as mouse body. c) Apply aerated lung vs everything else

473 threshold to scan inside ROI. d) Perform a series of computer operations to remove everything but

474 the aerated lungs. e) Data analysis on lungs, save lungs as ROI. f) Load lung only ROI. g) Obtain

475 Hounsfield Unit (HU) measurement using correction factor obtained from Distilled (DI) water

476 scan.

477 ***Lung Function Test:*** Pulmonary function assessment was performed using Plethysmography and

478 flexiVent (SCIREQ) systems following the manufacturers' protocols on all animals at the end of

479 the experiment.

480 ***Western Blot***: For Western blot, frozen tissues were lysed and homogenized in T-Per (Thermo

481 Fisher Scientific) with phosphatase and protease inhibitor (100 µl per 10 mg tissue, abcam,

482 ab201119). Protein content was measured with Nanodrop (280nm) and denaturation was

21

483 performed at 95°C for 5 min in the presence of 2-mercaptoethanol and Laemmli buffer. 20 µg

484 protein per lane was loaded onto a 4-20% gel (Bio-Rad) and samples were run at 50 mA followed

485 by transfer on PVDF membranes using the Trans-Blot Turbo Transfer System (biorad).

486 Membranes were washed, blocked in 5% dry milk (American bioInc) for 60 min followed by

487 incubation overnight (at 4°C) with primary antibody according to manufacturer's instruction (Cell

488 Signaling Technology, pSMAD3 (9520S) SMAD3 (9513S), both 1:1000). Signal was detected

489 using a donkey anti rabbit HRP conjugated antibody (Cytiva, 1:1000 for 1h at room temperature)

490 using enhanced chemiluminescence substrate (biorad). Quantification was done using ImageLab

491 software.

492 ***Ex vivo* Experiments, (Precision cut lung slices (PCLS))**

493 Mouse precision cut lung slices were generated as previously described (*48, 69, 70*). Mouse

494 lungs from both bleomycin (day 14) and Ad-TGF-β (day 21) models were used in parallel and

495 repeated accordingly. Briefly, low melting grade agarose (3 wt-%) was slowly injected via the

496 trachea to artificially inflate the lung. Lungs were cooled at 4°C for 15 minutes to allow gelling of

497 the agarose and then cut to a thickness of 150µm using a Compresstome (VF-300-0Z by

498 Precisionary®) at cutting speed of 6 µm/s and oscillation frequency of 5Hz. The PCLS were

499 cultured in a 24-well plate (Corning®) in 500µL DMEM-F12 no-phenol red containing 0.1% FBS

500 and 1% penicillin/streptomycin 37 °C, 5% CO_2 and 95% humidity. Treatment with saracatinib

501 (0.6µM), nintedanib (1µM), pirfenidone (1mM) or vehicle control, was administered in the first

502 24 hours after slicing. All media were changed daily, and lung slices were isolated 5 days after

503 treatment for analysis. Serial live imaging of lung slices by second harmonic generation

504 microscopy technique was performed before (Time; 0 hours) and after each treatment (Time; 120

505 hours) *(71)*. PCLS were fixed with 4% (weight/volume) paraformaldehyde overnight, and paraffin

506 embedded at 0h and 120h. 3μm sections were cut using a microtome, mounted on glass slides and

507 subjected to antigen retrieval. After deparaffinization and rehydration, staining was performed

508 according to standard protocols for Masson's Trichrome. Finally, samples were mounted using

509 mounting medium and covered with a cover slip. Microscopic scanning of the slides was

510 conducted in bright field with a Nikon inverted microscope at 20X magnification. 2 representative

511 images were acquired for each sample and at least 20 different random field of views were used

512 for collagen quantification. RNA was isolated from 5-6 replicated lung slices from each treatment

513 using miRNeasy Mini Kit (Qiagen) at time 0 and time 120 hours for all groups. mRNA levels of

514 fibrogenic genes were quantified by RT-qPCR and normalized to GAPDH expression. All

515 experimental groups were performed in a group of 6 technical replicates and repeated at least three

516 times.

517 ***Live/Dead assay:*** Cell viability in PCLS was assessed using LIVE/DEAD® Viability/Cytotoxicity

518 Kit following manufacturer's instruction (ThermoFisher Scientific; Cat. No. L3224). PCLS were

519 incubated with 2 μM Calcein AM and 2 μM Ethidium homodimer-1 (EthD-1) in 250 μm HBSS

520 for 30 min at 37 °C. They were then washed two times with HBSS and fixed with 10% buffered

521 formalin for 30 min at RT and washed. Samples were mounted on glass slides with ProLong®

522 Gold Antifade Mountant (ThermoFisher Scientific, Cat. No. P36930) and imaged using a Nikon

523 confocal microscope.

524 **Real-time Quantitative Reverse Transcription-Polymerase Chain Reaction for RNA**

525 **expression**

526 Relative expression of messenger RNA from all *in vitro*, *in vivo* and *ex vivo* experiments

527 were determined by real-time quantitative reverse transcription-polymerase chain reaction (RT-

528 qPCR) on Viia7 1.0 Real-Time PCR system using TaqMan gene expression assays. Reverse

23

529   transcription with random primers and subsequent PCR were performed with TaqMan RNA-to-

530   CT 1-Step Kit (Applied Biosystems). Raw data for cycle threshold (Ct) values were calculated

531   using the ViiA7 v.1 software with automatically set baseline. The results were analyzed by the

532   ΔΔCt method and GAPDH (Glyceraldehyde 3-phosphate dehydrogenase) was used as a

533   housekeeping gene. Fold change was calculated by taking the average over all the control samples

534   as the baseline. All the probes used in this study were purchased from Thermo Fisher Scientific.

535   **Connectivity mapping**

536   The connectivity mapping has been used previously by us and others *(22, 32, 72)* and the

537   pipeline utilized here has been recently described(*26*). Briefly, to obtain compound signatures,

538   A549 and MCF7 cell lines were exposed for 7 hours to two concentrations (3x IC50 and 10x IC50)

539   of compounds made available by AstraZeneca, followed by RNA extraction and RNASeq analysis

540   (single end, read length 49bp at BGI Genomics). A disease library was generated by collating

541   disease signatures from publicly available databases and consisted of 764 signatures representing

542   310 different diseases. IPF disease signatures were obtained from GSE24206 *(34)* and GSE44723

543   *(35)*. Disease signatures were compared to compound signatures, quantifying the extent of their

544   induced expression change using a modified Kolmogorov-Smirnov score to determine a single

545   connectivity score. The adjusted score reflects the specificity of the connection and allows for

546   better prioritization of disease connections. Connectivity scores were considered significant at

547   FDR < 0.01. Leading edge enrichment analysis was performed on the condition which showed the

548   highest connectivity (FDR 1.1 x 10^{-19}), ("Saracatinib_MCF7_Low_Dose" versus

549   "Advanced_IPF_explant_upper_lobe" obtained from GSE24206). Gene sets used in the

550   enrichment analysis were derived from a combination of publicly available sources including

551   Hallmark and KEA *(73)* .

Disease Enrichment Analysis

552

553　　For each compound signature, the full list of 764 disease signatures was rank ordered

554　according to ascending connectivity score. For each disease signature in the disease signature

555　library, we collated the relevant Disease Ontology Identifier (DOID), which reflects the disease

556　concept classification that best represents a given signature (*74*). For each DOID that has at least

557　three corresponding disease signatures, we calculated a signed running sum enrichment score,

558　which reflects whether that DOID is over-represented at the extreme ends of the ranked disease

559　list that has been ordered according to connectivity with a specific compound signature. DOID

560　enrichments with a positive score indicate a disease with multiple individual disease signatures at

561　the top of the ordered list i.e., diseases that are expected to be "normalized" by a given compound.

562　Statistical significance of DEA scores is based on comparison to a distribution of 1000 permuted

563　null scores, generated by calculating scores from randomized DOID sets that contain an equivalent

564　number of disease signatures to the true set being evaluated. Raw p-values are adjusted using the

565　Benjamini-Hochberg method of controlling the false discovery rate.

RNA sequencing

566

567　　NHLFs were treated with drugs or vehicle controls with and without TGF-β (10 conditions:

568　3 replicates each of vehicle A + media; vehicle A + TGF-β; saracatinib + TGF-β; nintedanib +

569　TGF-β; pirfenidone + TGF-β; saracatinib + vehicle B; nintedanib+ vehicle B; pirfenidone +

570　vehicle B; vehicle A + vehicle B; media + vehicle B). Total RNA was extracted with miRNeasy

571　Mini Kit (Qiagen-217004) according to the manufacturer's instructions. The purity of the RNA

572　was verified using a NanoDrop at 260 nm, and the quality of the RNA was assessed using the

573　Agilent 2100 Bioanalyzer (Agilent Technologies). Libraries were prepared using KAPA Stranded

574　mRNA-Seq Kit. mRNA was enriched by ribosomal RNA depletion. Library quality was checked

25

575   using Agilent TapeStation analyzer and sequencing was performed with NovaSeq (2X100, 25 M

576   reads per sample). FastQC files were generated and trimmed

577   (https://www.bioinformatics.babraham.ac.uk/projects/trim_galore/) and quality review was

578   performed by FastQC (http://www.bioinformatics.babraham.ac.uk/projects/fastqc/) before and

579   after quality trim. Reads were aligned with STAR aligner (version 2.6.1d, using the default

580   settings) to the HG38 human genome and ENSEMBL94 annotation GTF file. After alignment and

581   summarization with featureCounts of the Subread package (feature Counts release 1.6.3 and picard

582   version 2.18.21), samples were normalized using voom (limma package) and differential

583   expression was carried out with limma *(75)* implemented in R.

584   Mouse lungs were isolated from bleomycin and TGF-β mice models (8 conditions: 5

585   replicates each of bleomycin + vehicle, bleomycin + saracatinib, saline + vehicle, saline +

586   saracatinib, TGF-β + vehicle, TGF-β + saracatinib, empty vector + vehicle, empty vector +

587   saracatinib). Total RNA was extracted with miRNeasy Mini Kit (Qiagen-217004) and libraries

588   were prepared as above. Reads were mapped to reference genome mm9 by STAR/3.6.1d *(76)*

589   aligner supplemented with corresponding splice junction file Muc_musculus.GRCm38.96.gtf. At

590   least 90% of reads from each sample were mapped. Duplicates were removed by Picard2.20.2

591   MarkDuplicates (https://broadinstitute.github.io/picard/), read counts for each gene were obtained

592   by Subread/1.6.3 featureCounts *(77),* and gene annotations were obtained by biomaRt. Differential

593   expression gene analysis was performed with edgeR *(78)* and limma *(75)*. Low-expressed genes

594   were first filtered when counts were no more than 10 in at least 5 samples. After TMM

595   normalization, multidimensional scaling plots were used to explore sample similarities in an

596   unsupervised manner. FDR adjusted p-value < 0.05 was used as the cut-off (Benjamini-Hochberg

597   method).

26

Gene set enrichment analysis

Differentially expressed genes in TGF-β treated NHLFs treated with nintedanib and saracatinib were used for pathway enrichment by GSEA (http://software.broadinstitute.org/gsea/msigdb/annotate.jsp). Differentially expressed genes (adj. p-value < 0.05) were included in the enrichment analysis in Fig 2I and Table S2. There were no pathways enriched by nintedanib when including differentially expressed genes with an adjusted p-value < 0.05, therefore, we included genes with an adjusted p-value < 0.1 for both saracatinib and nintedanib for the purposes of this analysis (Figure S4B). The up-regulated and down-regulated gene sets for each drug treatment were used separately. The computed overlaps of each gene set were enriched against the Hallmark and KEGG gene sets from the MSigDB at FDR < 0.05.

Gene set enrichment analysis for both bleomycin and Ad-TGF-β mouse models was carried out using Camera *(79)*, against Hallmark (mouse_H_v5p2.rdata) and KEGG (mouse_c2_v5p2.rdata) datasets. Gene sets with FDR <0.05 were plotted using ggplot2.

Network analysis of mouse models

Protein-encoding gene interaction network analysis was carried out using Cytoscape v3.7.1 (*80*) with StringAPP plugin *(81)*. Breakdown into sub-networks was achieved by clusterMaker plugin MCL cluster function with inflation set at 2.5. Functional enrichment analysis of each cluster was performed using STRING enrichment against a collection of gene set databases including Gene Ontology, KEGG, and Reactome.

Statistics

For *in vitro* and *in vivo* assays statistical analysis was performed by GraphPad Prism version 8.1.2. Results were analyzed by Mann–Whitney *U* test for comparisons of two groups

27

621   when sample data were not normally distributed, by unpaired Student's *t*-test for comparisons of

622   two groups with normal distribution, and by one-way ANOVA with Student–Newman–Keuls *post*

623   *hoc* test for pairwise comparisons of three or more groups or more than 10 per group. Efficacy

624   experiments were designed for ten-fifteen animals in the control and treated groups, to allow for

625   82% power to detect a difference of 20% between the two groups at a statistical significance level

626   of 0.05, but the actual size of groups differed because of mortality. All data is presented as (means+

627   SEM) and the differences were considered statistically significant at $P < 0.05$.

628

629   **References**

630   1.   L. Richeldi, H. R. Collard, M. G. Jones, Idiopathic pulmonary fibrosis. *Lancet* **389**, 1941-

631   1952 (2017).

632   2.   F. J. Martinez, A. Chisholm, H. R. Collard, K. R. Flaherty, J. Myers, G. Raghu, S. L. Walsh,

633   E. S. White, L. Richeldi, The diagnosis of idiopathic pulmonary fibrosis: current and future

634   approaches. *Lancet Respir Med* **5**, 61-71 (2017).

635   3.   D. J. Lederer, F. J. Martinez, Idiopathic Pulmonary Fibrosis. *N Engl J Med* **379**, 797-798

636   (2018).

637   4.   G. Raghu, S. Y. Chen, W. S. Yeh, B. Maroni, Q. Li, Y. C. Lee, H. R. Collard, Idiopathic

638   pulmonary fibrosis in US Medicare beneficiaries aged 65 years and older: incidence,

639   prevalence, and survival, 2001-11. *Lancet Respir Med* **2**, 566-572 (2014).

640   5.   A. S. Lee, I. Mira-Avendano, J. H. Ryu, C. E. Daniels, The burden of idiopathic pulmonary

641   fibrosis: an unmet public health need. *Respir Med* **108**, 955-967 (2014).

6. T. M. Maher, E. Bendstrup, L. Dron, J. Langley, G. Smith, J. M. Khalid, H. Patel, M. Kreuter, Global incidence and prevalence of idiopathic pulmonary fibrosis. *Respir Res* **22**, 197 (2021).

7. A. L. Olson, J. J. Swigris, Idiopathic pulmonary fibrosis: diagnosis and epidemiology. *Clinics in chest medicine* **33**, 41-50 (2012).

8. M. A. Seibold, A. L. Wise, M. C. Speer, M. P. Steele, K. K. Brown, J. E. Loyd, T. E. Fingerlin, W. Zhang, G. Gudmundsson, S. D. Groshong, C. M. Evans, S. Garantziotis, K. B. Adler, B. F. Dickey, R. M. du Bois, I. V. Yang, A. Herron, D. Kervitsky, J. L. Talbert, C. Markin, J. Park, A. L. Crews, S. H. Slifer, S. Auerbach, M. G. Roy, J. Lin, C. E. Hennessy, M. I. Schwarz, D. A. Schwartz, A common MUC5B promoter polymorphism and pulmonary fibrosis. *N Eng J Med* **364**, 1503-1512 (2011).

9. M. Y. Armanios, J. J. Chen, J. D. Cogan, J. K. Alder, R. G. Ingersoll, C. Markin, W. E. Lawson, M. Xie, I. Vulto, J. A. Phillips, 3rd, P. M. Lansdorp, C. W. Greider, J. E. Loyd, Telomerase mutations in families with idiopathic pulmonary fibrosis. *N Engl J Med* **356**, 1317-1326 (2007).

10. T. E. King, Jr., A. Pardo, M. Selman, Idiopathic pulmonary fibrosis. *Lancet* **378**, 1949-1961 (2011).

11. T. A. Wynn, Integrating mechanisms of pulmonary fibrosis. *The Journal of experimental medicine* **208**, 1339-1350 (2011).

12. V. J. Thannickal, C. A. Henke, J. C. Horowitz, P. W. Noble, J. Roman, P. J. Sime, Y. Zhou, R. G. Wells, E. S. White, D. J. Tschumperlin, Matrix biology of idiopathic pulmonary fibrosis: a workshop report of the national heart, lung, and blood institute. *Am J Pathol* **184**, 1643-1651 (2014).

29

665   13.   R. Amanchy, J. Zhong, R. Hong, J. H. Kim, M. Gucek, R. N. Cole, H. Molina, A. Pandey,

666   Identification of c-Src tyrosine kinase substrates in platelet-derived growth factor receptor

667   signaling. *Mol Oncol* **3**, 439-450 (2009).

668   14.   G. M. Twamley-Stein, R. Pepperkok, W. Ansorge, S. A. Courtneidge, The Src family

669   tyrosine kinases are required for platelet-derived growth factor-mediated signal

670   transduction in NIH 3T3 cells. *Proc Natl Acad Sci U S A* **90**, 7696-7700 (1993).

671   15.   A. G. Tatosyan, O. A. Mizenina, Kinases of the Src family: structure and functions.

672   *Biochemistry (Mosc)* **65**, 49-58 (2000).

673   16.   M. Hu, P. Che, X. Han, G. Q. Cai, G. Liu, V. Antony, T. Luckhardt, G. P. Siegal, Y. Zhou,

674   R. M. Liu, L. P. Desai, P. J. O'Reilly, V. J. Thannickal, Q. Ding, Therapeutic targeting of

675   SRC kinase in myofibroblast differentiation and pulmonary fibrosis. *J Pharmacol Exp Ther*

676   **351**, 87-95 (2014).

677   17.   G. Hughes, H. Toellner, H. Morris, C. Leonard, N. Chaudhuri, Real World Experiences:

678   Pirfenidone and Nintedanib are Effective and Well Tolerated Treatments for Idiopathic

679   Pulmonary Fibrosis. *J Clin Med* **5**, (2016).

680   18.   L. Richeldi, R. M. du Bois, G. Raghu, A. Azuma, K. K. Brown, U. Costabel, V. Cottin, K.

681   R. Flaherty, D. M. Hansell, Y. Inoue, D. S. Kim, M. Kolb, A. G. Nicholson, P. W. Noble,

682   M. Selman, H. Taniguchi, M. Brun, F. Le Maulf, M. Girard, S. Stowasser, R. Schlenker-

683   Herceg, B. Disse, H. R. Collard, I. T. Investigators, Efficacy and safety of nintedanib in

684   idiopathic pulmonary fibrosis. *N Engl J Med* **370**, 2071-2082 (2014).

685   19.   T. E. King, Jr., W. Z. Bradford, S. Castro-Bernardini, E. A. Fagan, I. Glaspole, M. K.

686   Glassberg, E. Gorina, P. M. Hopkins, D. Kardatzke, L. Lancaster, D. J. Lederer, S. D.

687   Nathan, C. A. Pereira, S. A. Sahn, R. Sussman, J. J. Swigris, P. W. Noble, A. S. Group, A

30

688   phase 3 trial of pirfenidone in patients with idiopathic pulmonary fibrosis. *N Engl J Med*

689   **370**, 2083-2092 (2014).

690   20.   T. Corte, F. Bonella, B. Crestani, M. G. Demedts, L. Richeldi, C. Coeck, K. Pelling, M.

691   Quaresma, J. A. Lasky, Safety, tolerability and appropriate use of nintedanib in idiopathic

692   pulmonary fibrosis. *Respir Res* **16**, 116 (2015).

693   21.   F. Varone, G. Sgalla, B. Iovene, T. Bruni, L. Richeldi, Nintedanib for the treatment of

694   idiopathic pulmonary fibrosis. *Expert Opin Pharmacother* **19**, 167-175 (2018).

695   22.   J. T. Dudley, M. Sirota, M. Shenoy, R. K. Pai, S. Roedder, A. P. Chiang, A. A. Morgan,

696   M. M. Sarwal, P. J. Pasricha, A. J. Butte, Computational repositioning of the anticonvulsant

697   topiramate for inflammatory bowel disease. *Sci Transl Med* **3**, 96ra76 (2011).

698   23.   M. Sirota, J. T. Dudley, J. Kim, A. P. Chiang, A. A. Morgan, A. Sweet-Cordero, J. Sage,

699   A. J. Butte, Discovery and preclinical validation of drug indications using compendia of

700   public gene expression data. *Sci Transl Med* **3**, 96ra77 (2011).

701   24.   A. M. Brum, J. van de Peppel, C. S. van der Leije, M. Schreuders-Koedam, M. Eijken, B.

702   C. van der Eerden, J. P. van Leeuwen, Connectivity Map-based discovery of parbendazole

703   reveals targetable human osteogenic pathway. *Proc Natl Acad Sci U S A* **112**, 12711-12716

704   (2015).

705   25.   V. van Noort, S. Scholch, M. Iskar, G. Zeller, K. Ostertag, C. Schweitzer, K. Werner, J.

706   Weitz, M. Koch, P. Bork, Novel drug candidates for the treatment of metastatic colorectal

707   cancer through global inverse gene-expression profiling. *Cancer Res* **74**, 5690-5699

708   (2014).

709   26.   D. Bhattacharya, C. Becker, B. Readhead, N. Goossens, J. Novik, M. I. Fiel, L. P. Cousens,

710   B. Magnusson, A. Backmark, R. Hicks, J. T. Dudley, S. L. Friedman, Repositioning of a

novel GABA-B receptor agonist, AZD3355 (Lesogaberan), for the treatment of non-alcoholic steatohepatitis. *Sci Rep* **11**, 20827 (2021).

27. Y. M. Chang, L. Bai, S. Liu, J. C. Yang, H. J. Kung, C. P. Evans, Src family kinase oncogenic potential and pathways in prostate cancer as revealed by AZD0530. *Oncogene* **27**, 6365-6375 (2008).

28. T. P. Green, M. Fennell, R. Whittaker, J. Curwen, V. Jacobs, J. Allen, A. Logie, J. Hargreaves, D. M. Hickinson, R. W. Wilkinson, P. Elvin, B. Boyer, N. Carragher, P. A. Ple, A. Bermingham, G. A. Holdgate, W. H. Ward, L. F. Hennequin, B. R. Davies, G. F. Costello, Preclinical anticancer activity of the potent, oral Src inhibitor AZD0530. *Mol Oncol* **3**, 248-261 (2009).

29. J. Baselga, A. Cervantes, E. Martinelli, I. Chirivella, K. Hoekman, H. I. Hurwitz, D. I. Jodrell, P. Hamberg, E. Casado, P. Elvin, A. Swaisland, R. Iacona, J. Tabernero, Phase I safety, pharmacokinetics, and inhibition of SRC activity study of saracatinib in patients with solid tumors. *Clin Cancer Res* **16**, 4876-4883 (2010).

30. F. Ahangari, C. Becker, D. Foster, M. Chioccioli, M. Nelson, K. Beke, C. Meador, X. Wang, K. Corell, H. Roybal, G. Deluliis, K. Rose, J. C. Schupp, Q. Li, T. Adams, Y. Aschner, L. Lilli, B. Readhead, L. Cousens, J. Dudley, N. Kaminski, G. P. Downey, Saracatinib Is a Potential Novel Therapeutic for Pulmonary Fibrosis. *Am J Resp Crit Care* **201**, (2020).

31. J. Lamb, E. D. Crawford, D. Peck, J. W. Modell, I. C. Blat, M. J. Wrobel, J. Lerner, J. P. Brunet, A. Subramanian, K. N. Ross, M. Reich, H. Hieronymus, G. Wei, S. A. Armstrong, S. J. Haggarty, P. A. Clemons, R. Wei, S. A. Carr, E. S. Lander, T. R. Golub, The

733 Connectivity Map: using gene-expression signatures to connect small molecules, genes,

734 and disease. *Science* **313**, 1929-1935 (2006).

735 32. A. Subramanian, R. Narayan, S. M. Corsello, D. D. Peck, T. E. Natoli, X. Lu, J. Gould, J.

736 F. Davis, A. A. Tubelli, J. K. Asiedu, D. L. Lahr, J. E. Hirschman, Z. Liu, M. Donahue, B.

737 Julian, M. Khan, D. Wadden, I. C. Smith, D. Lam, A. Liberzon, C. Toder, M. Bagul, M.

738 Orzechowski, O. M. Enache, F. Piccioni, S. A. Johnson, N. J. Lyons, A. H. Berger, A. F.

739 Shamji, A. N. Brooks, A. Vrcic, C. Flynn, J. Rosains, D. Y. Takeda, R. Hu, D. Davison, J.

740 Lamb, K. Ardlie, L. Hogstrom, P. Greenside, N. S. Gray, P. A. Clemons, S. Silver, X. Wu,

741 W. N. Zhao, W. Read-Button, X. Wu, S. J. Haggarty, L. V. Ronco, J. S. Boehm, S. L.

742 Schreiber, J. G. Doench, J. A. Bittker, D. E. Root, B. Wong, T. R. Golub, A Next

743 Generation Connectivity Map: L1000 Platform and the First 1,000,000 Profiles. *Cell* **171**,

744 1437-1452 e1417 (2017).

745 33. Z. Wang, C. D. Monteiro, K. M. Jagodnik, N. F. Fernandez, G. W. Gundersen, A. D.

746 Rouillard, S. L. Jenkins, A. S. Feldmann, K. S. Hu, M. G. McDermott, Q. Duan, N. R.

747 Clark, M. R. Jones, Y. Kou, T. Goff, H. Woodland, F. M. R. Amaral, G. L. Szeto, O. Fuchs,

748 S. M. Schussler-Fiorenza Rose, S. Sharma, U. Schwartz, X. B. Bausela, M. Szymkiewicz,

749 V. Maroulis, A. Salykin, C. M. Barra, C. D. Kruth, N. J. Bongio, V. Mathur, R. D. Todoric,

750 U. E. Rubin, A. Malatras, C. T. Fulp, J. A. Galindo, R. Motiejunaite, C. Juschke, P. C.

751 Dishuck, K. Lahl, M. Jafari, S. Aibar, A. Zaravinos, L. H. Steenhuizen, L. R. Allison, P.

752 Gamallo, F. de Andres Segura, T. Dae Devlin, V. Perez-Garcia, A. Ma'ayan, Extraction

753 and analysis of signatures from the Gene Expression Omnibus by the crowd. *Nat Commun*

754 **7**, 12846 (2016).

755 34. E. B. Meltzer, W. T. Barry, T. A. D'Amico, R. D. Davis, S. S. Lin, M. W. Onaitis, L. D.
756   Morrison, T. A. Sporn, M. P. Steele, P. W. Noble, Bayesian probit regression model for
757   the diagnosis of pulmonary fibrosis: proof-of-principle. *BMC Med Genomics* **4**, 70 (2011).

758 35. R. Peng, S. Sridhar, G. Tyagi, J. E. Phillips, R. Garrido, P. Harris, L. Burns, L. Renteria, J.
759   Woods, L. Chen, J. Allard, P. Ravindran, H. Bitter, Z. Liang, C. M. Hogaboam, C. Kitson,
760   D. C. Budd, J. S. Fine, C. M. Bauer, C. S. Stevenson, Bleomycin induces molecular
761   changes directly relevant to idiopathic pulmonary fibrosis: a model for "active" disease.
762   *PLoS One* **8**, e59348 (2013).

763 36. J. Xiong, J. S. Wu, S. S. Mao, X. N. Yu, X. X. Huang, Effect of saracatinib on pulmonary
764   metastases from hepatocellular carcinoma. *Oncol Rep* **36**, 1483-1490 (2016).

765 37. J. Jin, S. Togo, K. Kadoya, M. Tulafu, Y. Namba, M. Iwai, J. Watanabe, K. Nagahama, T.
766   Okabe, M. Hidayat, Y. Kodama, H. Kitamura, T. Ogura, N. Kitamura, K. Ikeo, S. Sasaki,
767   S. Tominaga, K. Takahashi, Pirfenidone attenuates lung fibrotic fibroblast responses to
768   transforming growth factor-beta1. *Respir Res* **20**, 119 (2019).

769 38. J. Huang, C. Beyer, K. Palumbo-Zerr, Y. Zhang, A. Ramming, A. Distler, K. Gelse, O.
770   Distler, G. Schett, L. Wollin, J. H. Distler, Nintedanib inhibits fibroblast activation and
771   ameliorates fibrosis in preclinical models of systemic sclerosis. *Ann Rheum Dis* **75**, 883-
772   890 (2016).

773 39. L. Wollin, D. Togbe, B. Ryffel, Effects of Nintedanib in an Animal Model of Liver
774   Fibrosis. *Biomed Res Int* **2020**, 3867198 (2020).

775 40. S. I. Rothschild, Clinical potential of nintedanib for the second-line treatment of advanced
776   non-small-cell lung cancer: current evidence. *Lung Cancer (Auckl)* **5**, 51-57 (2014).

34

777   41.   K. E. Hostettler, J. Zhong, E. Papakonstantinou, G. Karakiulakis, M. Tamm, P. Seidel, Q.

778   Sun, J. Mandal, D. Lardinois, C. Lambers, M. Roth, Anti-fibrotic effects of nintedanib in

779   lung fibroblasts derived from patients with idiopathic pulmonary fibrosis. *Respir Res* **15**,

780   157 (2014).

781   42.   C. J. Schaefer, D. W. Ruhrmund, L. Pan, S. D. Seiwert, K. Kossen, Antifibrotic activities

782   of pirfenidone in animal models. *Eur Respir Rev* **20**, 85-97 (2011).

783   43.   Y. Y. Lu, X. K. Zhao, L. Yu, F. Qi, B. Zhai, C. Q. Gao, Q. Ding, Interaction of Src and

784   Alpha-V Integrin Regulates Fibroblast Migration and Modulates Lung Fibrosis in A

785   Preclinical Model of Lung Fibrosis. *Sci Rep* **7**, 46357 (2017).

786   44.   B. B. Moore, C. M. Hogaboam, Murine models of pulmonary fibrosis. *Am J Physiol Lung*

787   *Cell Mol Physiol* **294**, L152-160 (2008).

788   45.   P. J. Sime, Z. Xing, F. L. Graham, K. G. Csaky, J. Gauldie, Adenovector-mediated gene

789   transfer of active transforming growth factor-beta1 induces prolonged severe fibrosis in rat

790   lung. *J Clin Invest* **100**, 768-776 (1997).

791   46.   N. Frangogiannis, Transforming growth factor-beta in tissue fibrosis. *The Journal of*

792   *experimental medicine* **217**, e20190103 (2020).

793   47.   K. C. Flanders, Smad3 as a mediator of the fibrotic response. *Int J Exp Pathol* **85**, 47-64

794   (2004).

795   48.   M. Lehmann, L. Buhl, H. N. Alsafadi, S. Klee, S. Hermann, K. Mutze, C. Ota, M. Lindner,

796   J. Behr, A. Hilgendorff, D. E. Wagner, M. Konigshoff, Differential effects of Nintedanib

797   and Pirfenidone on lung alveolar epithelial cell function in ex vivo murine and human lung

798   tissue cultures of pulmonary fibrosis. *Respir Res* **19**, 175 (2018).

35

799   49.   M. Cedilak, M. Banjanac, D. Belamaric, A. Paravic Radicevic, I. Faraho, K. Ilic, S. Cuzic,
800   I. Glojnaric, V. Erakovic Haber, M. Bosnar, Precision-cut lung slices from bleomycin
801   treated animals as a model for testing potential therapies for idiopathic pulmonary fibrosis.
802   *Pulm Pharmacol Ther* **55**, 75-83 (2019).

803   50.   G. Yu, G. H. Ibarra, N. Kaminski, Fibrosis: Lessons from OMICS analyses of the human
804   lung. *Matrix Biol* **68-69**, 422-434 (2018).

805   51.   M. G. Palfreyman, Human tissue in target identification and drug discovery. *Drug Discov*
806   *Today* **7**, 407-409 (2002).

807   52.   N. Shanks, R. Greek, J. Greek, Are animal models predictive for humans? *Philos Ethics*
808   *Humanit Med* **4**, 2 (2009).

809   53.   A. Musa, L. S. Ghoraie, S. D. Zhang, G. Glazko, O. Yli-Harja, M. Dehmer, B. Haibe-
810   Kains, F. Emmert-Streib, A review of connectivity map and computational approaches in
811   pharmacogenomics. *Brief Bioinform* **18**, 903 (2017).

812   54.   H. Li, C. Zhao, Y. Tian, J. Lu, G. Zhang, S. Liang, D. Chen, X. Liu, W. Kuang, M. Zhu,
813   Src family kinases and pulmonary fibrosis: A review. *Biomed Pharmacother* **127**, 110183
814   (2020).

815   55.   A. Ulsamer, Y. Wei, K. K. Kim, K. Tan, S. Wheeler, Y. Xi, R. S. Thies, H. A. Chapman,
816   Axin pathway activity regulates in vivo pY654-beta-catenin accumulation and pulmonary
817   fibrosis. *J Biol Chem* **287**, 5164-5172 (2012).

818   56.   Y. Aschner, A. P. Khalifah, N. Briones, C. Yamashita, L. Dolgonos, S. K. Young, M. N.
819   Campbell, D. W. Riches, E. F. Redente, W. J. Janssen, P. M. Henson, J. Sap, N. Vacaresse,
820   A. Kapus, C. A. McCulloch, R. L. Zemans, G. P. Downey, Protein tyrosine phosphatase

alpha mediates profibrotic signaling in lung fibroblasts through TGF-beta responsiveness. *Am J Pathol* **184**, 1489-1502 (2014).

57. Y. Aschner, M. Nelson, M. Brenner, H. Roybal, K. Beke, C. Meador, D. Foster, K. A. Correll, P. R. Reynolds, K. Anderson, E. F. Redente, J. Matsuda, D. W. H. Riches, S. D. Groshong, A. Pozzi, J. Sap, Q. Wang, D. Rajshankar, C. A. G. McCulloch, R. L. Zemans, G. P. Downey, Protein tyrosine phosphatase-alpha amplifies transforming growth factor-beta-dependent profibrotic signaling in lung fibroblasts. *Am J Physiol Lung Cell Mol Physiol* **319**, L294-L311 (2020).

58. T. J. Boggon, M. J. Eck, Structure and regulation of Src family kinases. *Oncogene* **23**, 7918-7927 (2004).

59. A. Tzouvelekis, G. Yu, C. L. Lino Cardenas, J. D. Herazo-Maya, R. Wang, T. Woolard, Y. Zhang, K. Sakamoto, H. Lee, J. S. Yi, G. DeIuliis, N. Xylourgidis, F. Ahangari, P. J. Lee, V. Aidinis, E. L. Herzog, R. Homer, A. M. Bennett, N. Kaminski, SH2 Domain-Containing Phosphatase-2 Is a Novel Antifibrotic Regulator in Pulmonary Fibrosis. *Am J Respir Crit Care Med* **195**, 500-514 (2017).

60. Y. Aschner, G. P. Downey, Transforming Growth Factor-beta: Master Regulator of the Respiratory System in Health and Disease. *Am J Respir Cell Mol Biol* **54**, 647-655 (2016).

61. N. Kaminski, J. D. Allard, J. F. Pittet, F. Zuo, M. J. Griffiths, D. Morris, X. Huang, D. Sheppard, R. A. Heller, Global analysis of gene expression in pulmonary fibrosis reveals distinct programs regulating lung inflammation and fibrosis. *Proc Natl Acad Sci U S A* **97**, 1778-1783 (2000).

62. A. Abdollahi, M. Li, G. Ping, C. Plathow, S. Domhan, F. Kiessling, L. B. Lee, G. McMahon, H. J. Grone, K. E. Lipson, P. E. Huber, Inhibition of platelet-derived growth

37

844   factor signaling attenuates pulmonary fibrosis. *The Journal of experimental medicine* **201**,

845   925-935 (2005).

846 63. L. Veracini, M. Franco, A. Boureux, V. Simon, S. Roche, C. Benistant, Two functionally

847   distinct pools of Src kinases for PDGF receptor signalling. *Biochem Soc Trans* **33**, 1313-

848   1315 (2005).

849 64. H. Xiao, X. Huang, S. Wang, Z. Liu, R. Dong, D. Song, H. Dai, Metformin ameliorates

850   bleomycin-induced pulmonary fibrosis in mice by suppressing IGF-1. *Am J Transl Res* **12**,

851   940-949 (2020).

852 65. R. D. Guzy, L. Li, C. Smith, S. J. Dorry, H. Y. Koo, L. Chen, D. M. Ornitz, Pulmonary

853   fibrosis requires cell-autonomous mesenchymal fibroblast growth factor (FGF) signaling.

854   *J Biol Chem* **292**, 10364-10378 (2017).

855 66. M. Imamura, J. S. Moon, K. P. Chung, K. Nakahira, T. Muthukumar, R. Shingarev, S. W.

856   Ryter, A. M. Choi, M. E. Choi, RIPK3 promotes kidney fibrosis via AKT-dependent ATP

857   citrate lyase. *JCI Insight* **3**, (2018).

858 67. D. J. Webb, K. Donais, L. A. Whitmore, S. M. Thomas, C. E. Turner, J. T. Parsons, A. F.

859   Horwitz, FAK-Src signalling through paxillin, ERK and MLCK regulates adhesion

860   disassembly. *Nat Cell Biol* **6**, 154-161 (2004).

861 68. D. V. Pechkovsky, A. K. Scaffidi, T. L. Hackett, J. Ballard, F. Shaheen, P. J. Thompson,

862   V. J. Thannickal, D. A. Knight, Transforming growth factor beta1 induces alphavbeta3

863   integrin expression in human lung fibroblasts via a beta3 integrin-, c-Src-, and p38 MAPK-

864   dependent pathway. *J Biol Chem* **283**, 12898-12908 (2008).

865 69. H. N. Alsafadi, C. A. Staab-Weijnitz, M. Lehmann, M. Lindner, B. Peschel, M.

866   Konigshoff, D. E. Wagner, An ex vivo model to induce early fibrosis-like changes in

38

human precision-cut lung slices. *Am J Physiol Lung Cell Mol Physiol* **312**, L896-L902 (2017).

70. F. E. Uhl, S. Vierkotten, D. E. Wagner, G. Burgstaller, R. Costa, I. Koch, M. Lindner, S. Meiners, O. Eickelberg, M. Konigshoff, Preclinical validation and imaging of Wnt-induced repair in human 3D lung tissue cultures. *Eur Respir J* **46**, 1150-1166 (2015).

71. Y. Liu, A. Keikhosravi, G. S. Mehta, C. R. Drifka, K. W. Eliceiri, Methods for Quantifying Fibrillar Collagen Alignment. *Methods Mol Biol* **1627**, 429-451 (2017).

72. J. T. Dudley, R. Tibshirani, T. Deshpande, A. J. Butte, Disease signatures are robust across tissues and experiments. *Mol Syst Biol* **5**, 307 (2009).

73. A. Lachmann, A. Ma'ayan, KEA: kinase enrichment analysis. *Bioinformatics* **25**, 684-686 (2009).

74. L. M. Schriml, E. Mitraka, J. Munro, B. Tauber, M. Schor, L. Nickle, V. Felix, L. Jeng, C. Bearer, R. Lichenstein, K. Bisordi, N. Campion, B. Hyman, D. Kurland, C. P. Oates, S. Kibbey, P. Sreekumar, C. Le, M. Giglio, C. Greene, Human Disease Ontology 2018 update: classification, content and workflow expansion. *Nucleic Acids Res* **47**, D955-D962 (2019).

75. M. E. Ritchie, B. Phipson, D. Wu, Y. Hu, C. W. Law, W. Shi, G. K. Smyth, limma powers differential expression analyses for RNA-sequencing and microarray studies. *Nucleic Acids Res* **43**, e47 (2015).

76. A. Dobin, C. A. Davis, F. Schlesinger, J. Drenkow, C. Zaleski, S. Jha, P. Batut, M. Chaisson, T. R. Gingeras, STAR: ultrafast universal RNA-seq aligner. *Bioinformatics* **29**, 15-21 (2013).

77. Y. Liao, G. K. Smyth, W. Shi, featureCounts: an efficient general purpose program for assigning sequence reads to genomic features. *Bioinformatics* **30**, 923-930 (2014).

78. M. D. Robinson, D. J. McCarthy, G. K. Smyth, edgeR: a Bioconductor package for differential expression analysis of digital gene expression data. *Bioinformatics* **26**, 139-140 (2010).

79. D. Wu, G. K. Smyth, Camera: a competitive gene set test accounting for inter-gene correlation. *Nucleic Acids Res* **40**, e133 (2012).

80. P. Shannon, A. Markiel, O. Ozier, N. S. Baliga, J. T. Wang, D. Ramage, N. Amin, B. Schwikowski, T. Ideker, Cytoscape: a software environment for integrated models of biomolecular interaction networks. *Genome Res* **13**, 2498-2504 (2003).

81. N. T. Doncheva, J. H. Morris, J. Gorodkin, L. J. Jensen, Cytoscape StringApp: Network Analysis and Visualization of Proteomics Data. *J Proteome Res* **18**, 623-632 (2019).

926

927

928

929

930

931

932

933

934

935 **Figures and Tables**

A

Drug Signatures	Disease Transcriptomic Library	Filtering and Secondary Analysis	Prioritization of Results

Data Production:
32 Compounds
2 Cell Lines
2 Dosages

QC Pre-Proessing and
Normalization
Sample Clustering
MDS/PCA Plots
Variance Partion

Condition specific drug
signatures:

Compound A: A549 Low Dose
Compound A: A549 High Dose
Compound A: MCF7 Low Dose
Compound A: MCF7 High Dose

Publicly available data from GEO

Disease Library

Top Inverse Connections

Disease Promiscuity Annotations

Disease Enrichment Analysis

Leading Edge Enrichment
Analysis

Novel Disease Indications

B

Drug Signature	DOID	Score	FDR	Disease Signatures	Position
Saracatinib: Low dose MCF7	50156: Idiopathic Pulmonary Fibrosis	0.53	9.26×10^{-2}	GSE24206: Advanced IPF (lung upper lobe) Female	14
				GSE24206: Advanced IPF (lung upper lobe) Male	36
				GSE24206: Advanced IPF (lung lower lobe) Female	44
				GSE44723: Lung fibroblasts (rapidly progressing fibrosis)	188
				GSE24206: Early IPF (lung upper lobe) Male	247
				GSE24206: Early IPF (lung lower lobe) Male	289
				GSE44723: Lung fibroblasts (slow progressing fibrosis)	355
				GSE24206: Advanced IPF (lung lower lobe) Male	361

C

Connectivity to GSE44

| Compound	Adjusted Score	FDR
Saracatinib	-2.09	6.79×10
Dasatinib	-1.88	4.96×10^{-6}
Bosutinib	-1.78	2.19×10^{-5}
Pirfenidone	1.33	8.87×10^{-3}
Nintedanib	-1.32	1.17×10^{-2}
NM-PP1	-1.28	1.47×10^{-2}

936

42

937 **Figure 1. Computational drug repurposing identifies saracatinib as a potential therapeutic**

938 **for IPF.**

939 **(A)** Schematic of the *in-silico* approach used to identify novel disease indications for compounds.

940 Drug signatures were obtained for 32 compounds in two different cell lines at two dosages. Each

941 drug signature was compared to a library of disease signatures generated from publicly available

942 data and a connectivity score was generated for each disease-compound pair. Filtering and

943 secondary analyses were carried out to identify novel disease indications for each of the

944 compounds. **(B)** Disease enrichment analysis results showing enrichment of DOID:50156/IPF

945 signatures among disease signatures that are transcriptomically connected to saracatinib. **(C)**

946 Connectivity scores between an IPF disease signature and publicly available drug signatures

947 (saracatinib, dasatinib, bosutinib, pirfenidone, nintedanib and NM-PP1; obtained from LINCS

948 L1000).

949

950

951

952

953

954

955

956

957

958

959

960

43

961

962

963

964

965

966

967

968

969

970

971

972

973

974

975

976

977

978

979

980

981

982

983

44
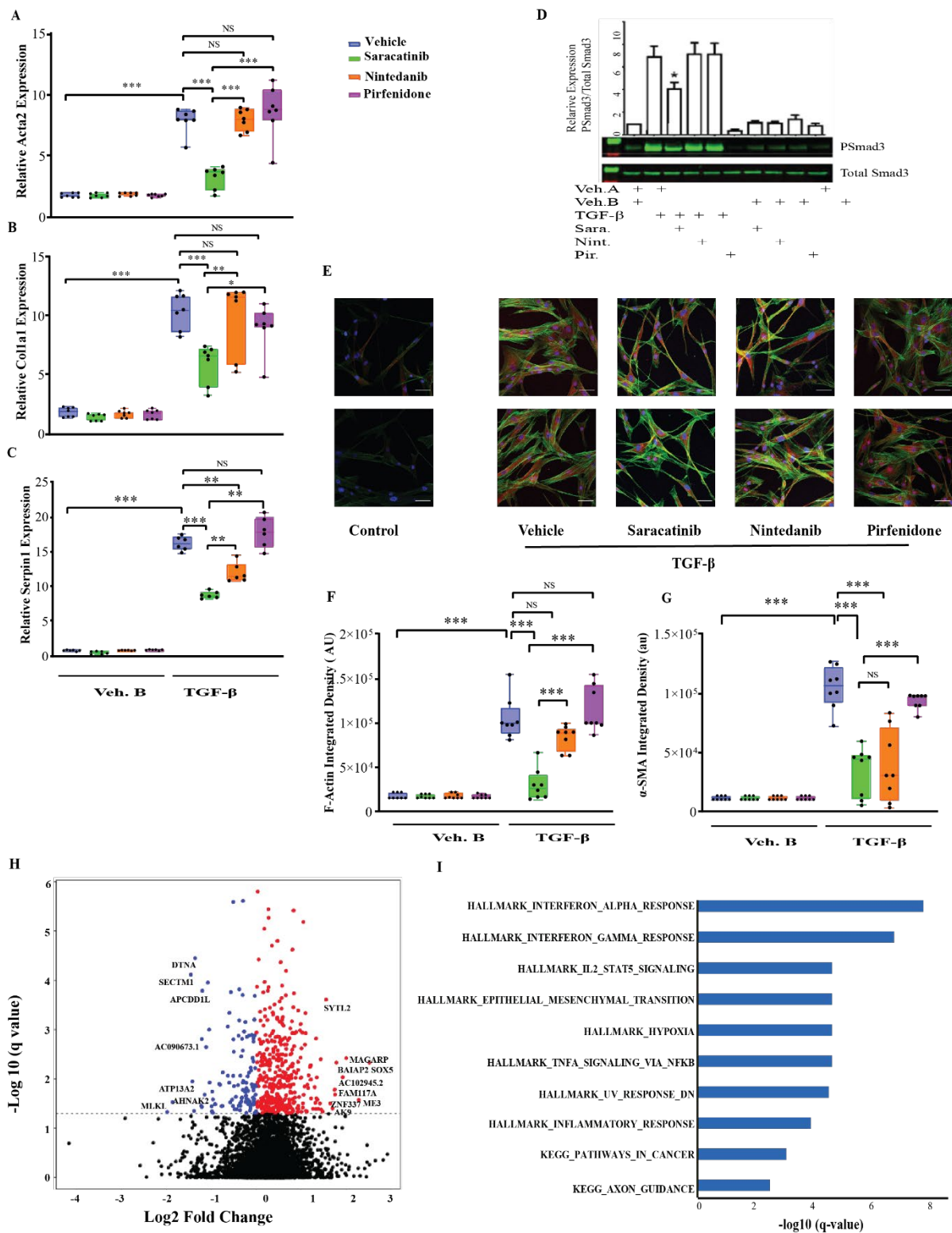
984 **Figure 2. Saracatinib inhibits TGF-β–induced phenotypic changes in human lung fibroblasts**

985 **(NHLFs).**

986 Cells were serum-starved overnight and then incubated with inhibitors (saracatinib: (0.3

987 μM), nintedanib: (1 μM), pirfenidone: (20 μg/ml) or Vehicle (DMSO)) for 60 min followed by

988 stimulation with human recombinant TGF-β (2 ng/ml) or vehicle control for the indicated times.**(A,**

989 **B and C)** RT-qPCR analysis for **(A)** *ACTA2* **(B)** *COL1A1* and **(C)** *SERPIN-1* (*Pie-1*), in the

990 indicated treatment groups of NHLF(means+ SEM), *P<0.05,**P<0.01,***P<0.001(n=6).**(D)**

991 Representative western blots showing saracatinib inhibits TGF-β-Induced phosphorylation of

992 Smad3 in human lung fibroblasts, data presented as means+ SEM, n=6, *P<0.05 **(E)**

993 Representative images of α-SMA staining (red) along with F-Actin (green) and DAPI (blue) show

994 fluorescent staining in human fibroblasts after TGF-β stimulation in the indicated treatment groups

995 using confocal microscopy. **(F)** and **(G)** Quantification of α-SMA and F-Actin staining shown as

996 integrated density, ***P<0.001. **(H)** Volcano plot showing genes that are differentially expressed

997 in cells treated with TGF-β and saracatinib compared to TGF-β alone (FDR<0.05, negative fold

998 change (blue) and positive fold change (red). **(I)** Functional enrichment of significantly

999 differentially expressed genes (FDR<0.05) in response to saracatinib (only top 10 gene sets shown.

1000 All gene sets shown are significant at FDR <0.05 and are from Hallmark (H) or Kegg (K).

1001

1002

1003

1004

1005

1006

1007

45
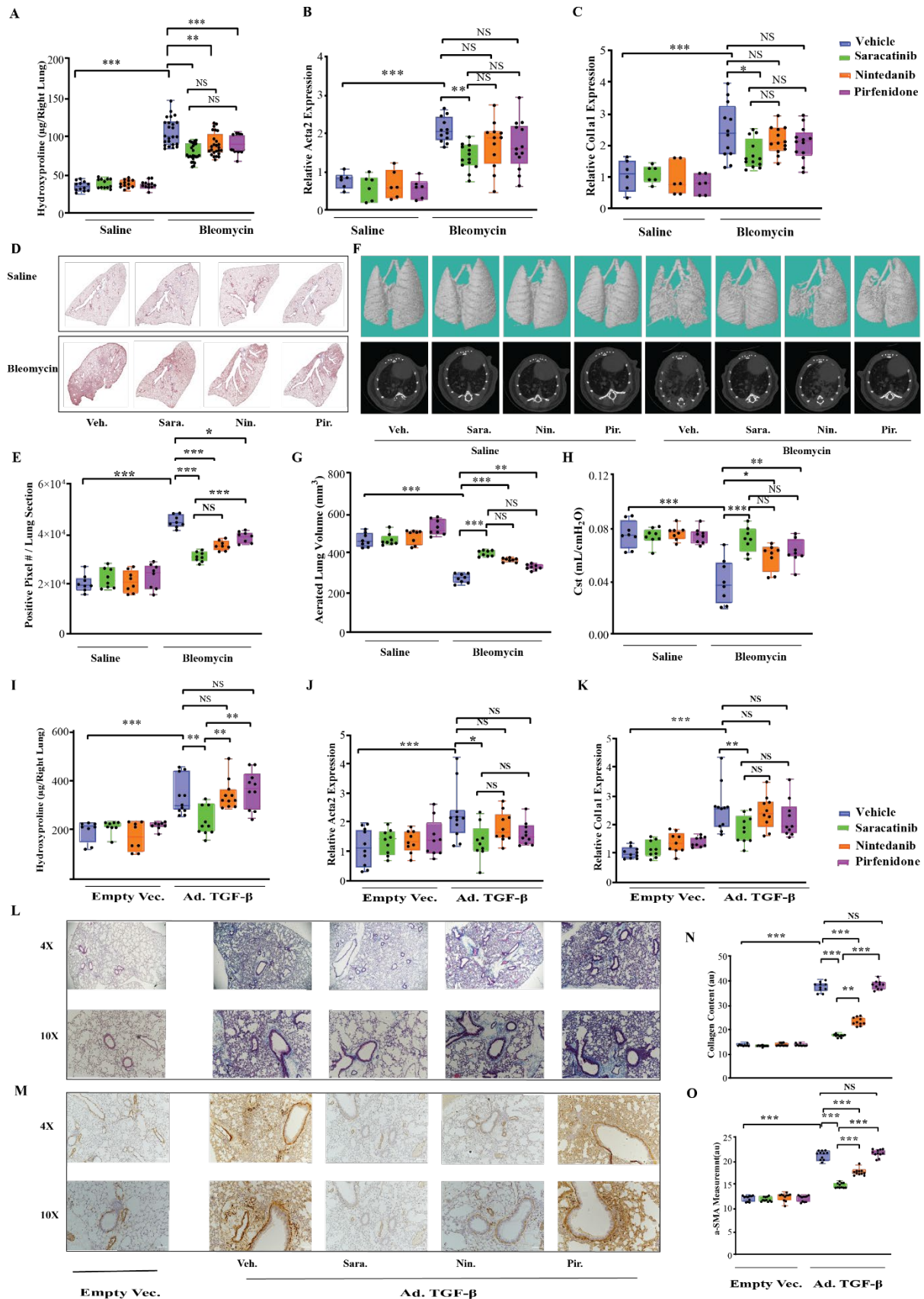
Figure 3. Saracatinib inhibits pulmonary fibrosis in bleomycin and adenovirus TGF-β mouse models.
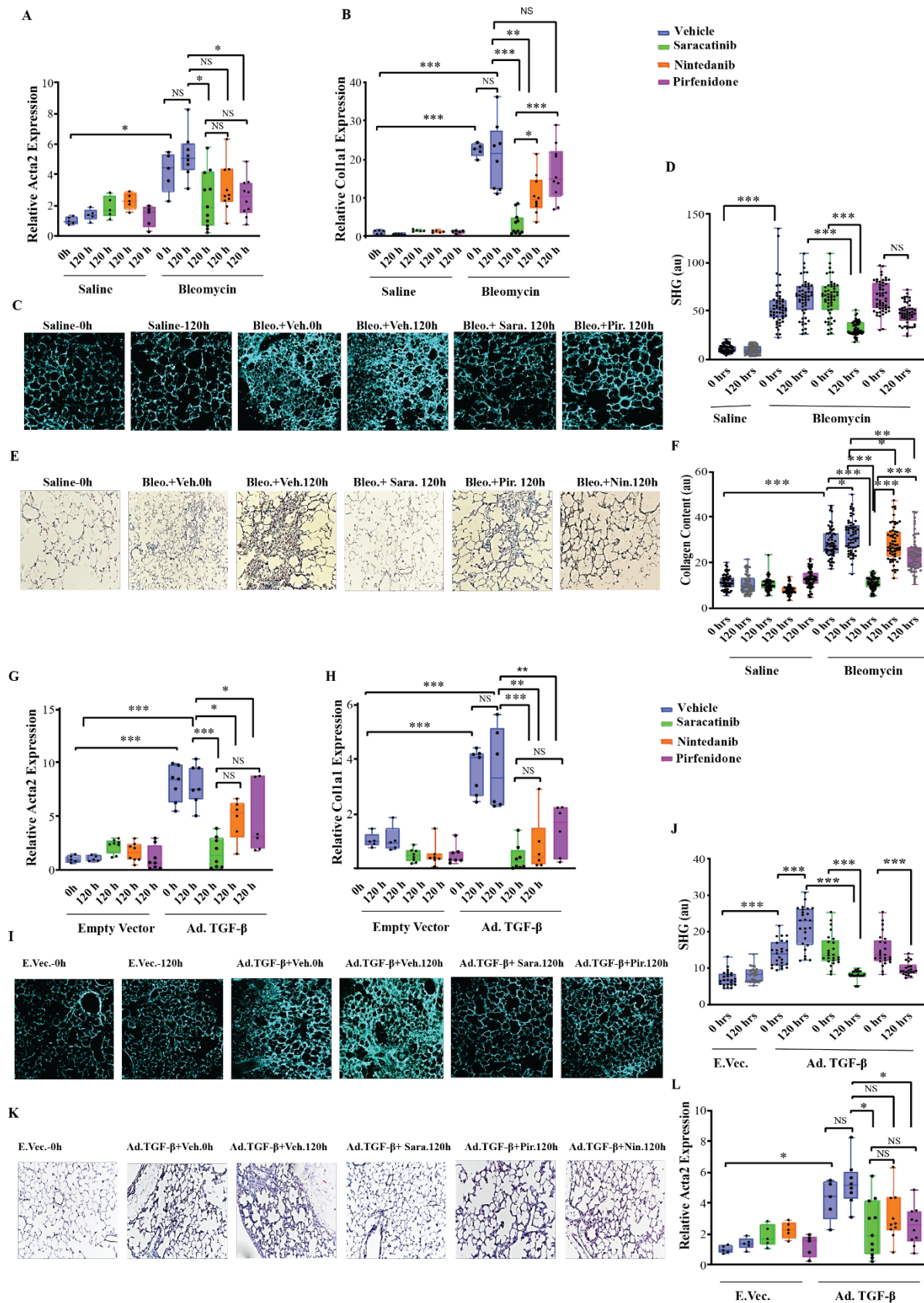
(A-H) Evaluation of bleomycin-induced lung fibrosis: (A) Quantitative analysis of hydroxyproline in lung homogenates from indicated groups of mice. Lung collagen content increased significantly in bleomycin-treated mice receiving vehicle control (fold change=2.9), **P < 0.01, ***P < 0.001. **(B and C)** RT-qPCR analysis on mouse lungs for **(B)** *Acta2* **(C)** *Col1a1* in the indicated treatment groups. **(D and E)** Representative images and quantitative measurements of Masson's Trichrome staining of lung sections in the indicated groups of mice. **(F and G)** Representative images (dorsal view of three -dimensional reconstructions and axial view) and quantifications of microCT on mouse lung tissues in the indicated groups. Gross abnormality resulting from bleomycin- induced lung fibrosis is alleviated after treatment. Aerated lung volume measurements showed a significant decrease in bleomycin-treated mice lung (p-value ≤0.001, fold change >2), while saracatinib and nintedanib significantly attenuated the bleomycin-induced radiographic alterations in lung parenchyma (p-value ≤0.001). **(H)** Lung compliance measurements of each mice lung at the end of the study in the indicated groups, shown as static compliance (Cst).

(I-O) Evaluation of Ad-TGF-β-induced lung fibrosis: (I) Quantitative analysis of hydroxyproline in lung homogenates from indicated groups of mice, the hydroxyproline assay revealed a significant increase in lung collagen content for mice receiving Ad-TGF-β (fold change=1.8, p-value ≤0.001) **(J and K)** RT-qPCR analysis on mouse lungs for **(J)** *Acta2* **(K)** *Col1a1* in the indicated treatment groups. **(L and N)** Representative images and quantification of Masson's Trichrome staining of lung sections in the indicated groups of mice. **(M and O)**

47

1057 Representative images and quantification of α-SMA staining of lung sections in the indicated

1058 groups of mice.

1059 All data is presented as (means+ SEM), *P <0.05, **P <0.01, ***P<0.001, (n=6 in controls and

1060 n≥12 in bleomycin and TGF-β treated groups).

1061

1062

1063

1064

1065

1066

1067

1068

1069

1070

1071

1072

1073

1074

1075

1076

1077

1078

1079

1080

48

1081

49
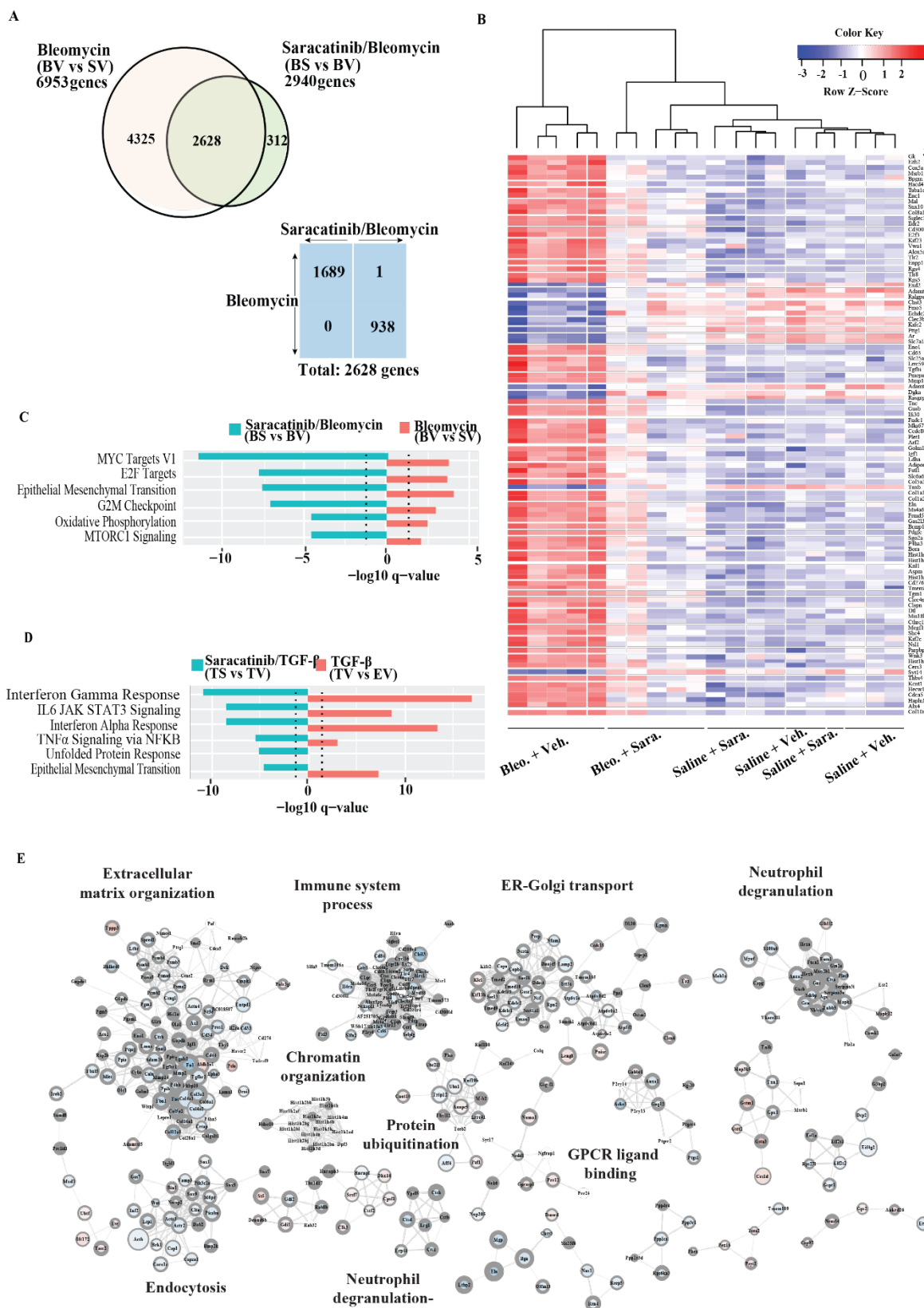
Figure 4. Saracatinib inhibits pulmonary fibrosis in *ex vivo* murine PCLS in bleomycin and Ad-TGF-β models.

Mouse precision cut lung slices (PCLS) were generated from both bleomycin (day 14) and Ad-TGF-β (day 21). Treatment with saracatinib (0.6μM), nintedanib (1μM), pirfenidone (1mM) or vehicle control, was administered in the first 24 hours after slicing (Time 0 hour). All lung slices were isolated 5 days after treatment for analysis (Time 120 hours).

(A-F) Effects of saracatinib, nintedanib and pirfenidone in PCLS isolated from bleomycin mice model of pulmonary fibrosis. **(A and B)** RT-qPCR analysis on mice PCLS in bleomycin model for *Acta2* and *Col1a1* at time 0 and 120 hours after indicated treatments. **(C and D)** Representative live images by second harmonic generation microscopy (SHG) and quantification assessments of PCLS samples at time 0 and 5 days (120 hours) after indicated treatments. **(E and F)** Representative images and quantification assessments of Masson's Trichrome staining of PCLS slides at time 0 and 5 days (120 hours) after indicated treatments.

(G-L) Effects of saracatinib, nintedanib and pirfenidone in PCLS isolated from Ad-TGF-β treated murine model of pulmonary fibrosis. **(G and H)** qRT-PCR analysis on murine PCLS in the Ad-TGF-β model for *Acta2* and *Col1a1* at time 0 and 120 hours after indicated treatments. **(I and J).** Representative live images using second harmonic generation microscopy (SHG) and quantification assessments of PCLS samples at time 0 and 5 days (120 hours) after indicated treatment. **(K and L)** Representative images and quantification assessments of Masson's Trichrome staining of PCLS samples at time 0 and 5 days (120 hours) after indicated treatment. All data is presented as (means+ SEM), P < 0.05, **P<0.01, ***P<0.001, (n≥6 in all groups).

50

1128

1129

1130

1131

1132

1133

1134

1135

1136

1137

1138

1139

1140

1141

1142

1143

1144

1145

1146

1147

1148

1149

1150

51

Figure 5. Saracatinib treatment results in reversal of transcriptional changes observed in IPF mouse models.

(A) Comparison of number and direction of significantly differentially expressed genes (FDR <0.05) in bleomycin, and bleomycin/saracatinib treatment groups. Bleomycin administration induced significant differential expression of almost 7000 genes (adj. p-value <0.05) in the bleomycin treatment group when compared the control group. Bleomycin-treated mice that also received saracatinib had significant changes in 2940 genes compared to mice treated with bleomycin alone. 2628 differentially expressed genes are common between treatment groups. Of these 1689 are upregulated by bleomycin and downregulated by saracatinib; and 938 are downregulated by bleomycin and upregulated by saracatinib. **(B)** Heatmap of top 100 differentially expressed genes (BS vs BV). **(C)** Top Hallmark GSEA in bleomycin murine experiments (adj. p-value <0.05) ranked by saracatinib effect. Blue bars show BS vs BV and red bars show BV vs SV. The positive or negative signs indicate logFC directions. **(D)** Top Hallmark GSEA in Ad-TGF-β experiments ranked by saracatinib effect (adj. p-value <0.05). Blue bars show TS vs TV and red bars TV vs EV. The positive or negative signs indicate logFC directions. **(E)** Cytoscape network analysis of common DE genes shared by both the bleomycin and TGF-β mouse models that are reversed by saracatinib. Node size - expression level; Node color – LogFC (red is up, blue is down); node border width – negative log adj. p-value. *Key: Bleomycin experimental conditions: SV: saline + vehicle; BV: bleomycin + vehicle; BS - bleomycin + saracatinib; BV vs SV - bleomycin effect; BS vs BV - saracatinib on bleomycin. Ad-TGF-β experimental conditions: EV: control + vehicle; TV: TGF-β + vehicle; TS: TGF-β + saracatinib; TV vs EV: TGF-β effect; TS vs TV: saracatinib on TGF-β.*

1174

			Enrichments: ↑ IPF, ↓ Saracatinib			Enrichments: ↓ IPF, ↑ Saracatinib		
Library	Gene Set	FDR	Genes in Overlap	F.C.	Gene Set	FDR	Genes in Overlap	F.C.
Hallmark	IFNγ response	1.79×10^{-12}	ADAR, CD74, HLA-A, HLA-B, HLA-DMA, HLA-G, ICAM1, IFI30, IFIT3, IFITM3, IRF1, LGALS3BP, LY6E, MT2A, MX1, MYD88, NFKBIA, PTPN6, SERPING1	9.48	Myc targets	3.47×10^{-9}	CCT2, DEK, DHX15, ERH, GLO1, HNRNPA1, IARS, LDHA, NPM1, PSMA6, RPL6, RPLP0, SLC25A3, YWHAQ	9.28
	EMT	5.94×10^{-11}	CAPG, COL1A1, COL4A2, COL6A2, CYR61, FLNA, FN1, GEM, HTRA1, ID2, IGFBP2, IGFBP4, SERPINE1, SERPINH1, TAGLN, TGFBI, VIM	8.54	Allograft rejection	1.35×10^{-4}	B2M, HIF1A, IFNGR1, MRPL3, NPM1, RPS3A, TIMP1	8.59
	TNFα signaling via NF-kB	4.03×10^{-10}	CCND1, CD83, CYR61, EGR1, FOSB, GEM, ICAM1, ID2, IER2, IRF1, JUNB, KDM6B, LAMB3, LIF, NFKBIA, SERPINE1, SLC2A3, ZFP36	7.88	Apoptosis	4.39×10^{-4}	CAV1, GPX3, IFNGR1, PPT1, TGFBR3, TIMP1, TXNIP	6.91
	Complement	2.50×10^{-8}	APOC1, C3, COL4A2, CSRP1, CTSD, CTSH, DUSP6, FN1, GNAI2, GNB2, IRF1, PFN1, SERPINE1, SERPING1, TIMP2	7.81	Inflammatory response	1.49×10^{-2}	ADM, HIF1A, LAMP3, NAMPT, TIMP1	6.08
	Coagulation	3.70×10^{-8}	APOC1, C3, CRIP2, CSRP1, CTSH, DUSP6, FN1, GNB2, HTRA1, SERPINE1, SERPING1, USP11	10.07	Reactive oxygen species	1.81×10^{-2}	GPX3, PRDX1, PRDX6	8.95
	INFα response	1.61×10^{-6}	ADAR, CD74, HLA-C, IFI30, IFIT3, IFITM3, IRF1, LGALS3BP, LY6E, MX1	9.03	Oxidative phosphorylation	1.84×10^{-2}	COX6C, COX7A2, LDHA, NDUFA4, SLC25A3, SLC25A5	3.98
	Allograft rejection	2.79×10^{-5}	CAPG, CD74, FLNA, HLA-A, HLA-DMA, HLA-E, HLA-G, ICAM1, LIF, PTPN6	6.67	Androgen response	3.27×10^{-2}	B2M, MYL12A, SGK1, SLC38A2	5.77
	Apical junction	4.75×10^{-5}	ACTB, ACTG1, ACTN4, CAP1, EVL, GNAI2, ICAM1, LAMB3, PFN1, TGFBI, VASP, ZYX	5.63	EMT	4.94×10^{-2}	CD59, GJA1, TGFBR3, TIMP1	3.70
KEA	RIPK3	3.42×10^{-6}	ACTB, ACTG1, ACTN4, FLNA, GNB2, HSPA8, RPS27, AUB52, UBB, VIM	8.31	MAP3K14	3.89×10^{-10}	HNRNPA1, HSPA1A, IARS, NPM1, RPL24, RPL4, RPL6, RPL7A, RPL10, RPS11, RPS23, RPS3A, RPS7	12.74
	MAP3K3	5.42×10^{-6}	ACTB, ACTG1, ACTN4, FLNA, GNAI2, GNB2, HSPA8, NFKBIA, RPS27, TUBA1C, UBA52, UBB, VIM	5.66	RIPK3	3.42×10^{-6}	CCt2, HNRNPA1, HSPA1A, PPP1CB, PPP1CC, PRDX1, SLC25A3, SLC25A5	12.17
	MAP3K1	1.56×10^{-5}	ACTB, ACTG1, FLNA, HSPA8, LGALS3BP, NFKBIA, RPL35, RPS27, UBA52, UBB, VIM	6.52	MAP3K1	1.71×10^{-3}	HSPA1A, RPL24, RPL4, RPS11, RPS23, SLC25A5	6.50
	MAP3K14	4.89×10^{-4}	ACTB, ACTG1, FAU, HSPA8, NFKBIA, RPL35, RPS10, RPS18, RPS20	4.82	MAP3K3	7.38×10^{-3}	CCT2, HSPA1A, IARS, PPP1CC, SLC25A5, YWHAQ	4.79

1175

1176 **Table 1. Leading edge enrichment analysis.**

1177 Enrichment analysis performed on leading edge of saracatinib drug signature versus IPF disease

1178 signature (GSE24206). The drug-disease pair which showed the highest connectivity was used for

1179 the analysis, namely "Saracatinib MCF7 Low Dose" versus "Advanced_IPF_explant_upper_lobe

1180 obtained from GSE24206". F.C.=Fold Change. Gene sets and overlapping genes are listed.

53

1181

Supplementary Materials

Figure S1. TGF-β induces Src activation in normal human lung fibroblasts.

Figure S2. Evaluation of the effects of two different doses of saracatinib, nintedanib and pirfenidone in TGF-β1-induced profibrotic gene expressions in normal human lung fibroblasts.

Figure S3. Saracatinib inhibits TGF-β1–induced phenotypic changes in primary human lung fibroblasts isolated from three different donors to confirm the consistency across donors.

Figure S4. Transcriptomic analysis revealed that both nintedanib and saracatinib target several common gene sets.

Figure S5. Mice receiving saracatinib treatment recovered their weight losses in both bleomycin and Ad-TGF-β mouse models.

Figure S6. Saracatinib inhibits *Col3a1* in bleomycin and Ad-TGF-β mouse models.

Figure S7. Representative images (Dorsal view of three-dimensional reconstructions and Axial view) of microCT on mouse lung tissues in bleomycin mice model in the indicated groups.

Figure S8. Representative images of lung tissues in Ad-TGF-β mouse model.

Figure S9. Western blot analysis of lung tissues identified saracatinib significantly inhibits Phospho-Smad3 signaling in both animal models of pulmonary fibrosis.

Figure S10. LIVE/DEAD® Viability/Cytotoxicity identified the viability of PCLS after 5 days in culture.

Figure S11. Enlarged version of Cytoscape network analysis of common differentially expressed genes shared by both the bleomycin and Ad-TGF-β mouse models that are reversed by saracatinib**.**

Table S1. Connection between IPF and saracatinib signature.

Table S2. Enrichment analysis of significantly differentially expressed genes.